Investigation of Carbohydrate Conformation in Solution and in Powders by Double-Quantum NMR

Sapna Ravindranathan,[†,‡] Xiaolong Feng,[†,§] Torgny Karlsson,[†] Göran Widmalm,[||] and Malcolm H. Levitt[†,*]

Contribution from the Physical Chemistry Division, Arrhenius Laboratory, University of Stockholm, S-10691 Sweden, and Department of Organic Chemistry, Arrhenius Laboratory, University of Stockholm, S-10691 Sweden

Received April 5, 1999. Revised Manuscript Received November 8, 1999

Abstract: Double-quantum heteronuclear local field NMR was applied to two $^{13}C_2$-labeled carbohydrate samples, [1,2-$^{13}C_2$]-glucose and methyl-α-D-[1,3-$^{13}C_2$]-glucose. The geometry of the H−^{13}C−^{13}C−H moiety was estimated using the evolution of double-quantum coherences under correlated heteronuclear dipolar interactions. For [1,2-$^{13}C_2$]-glucose, double-quantum techniques were used both in solution and solid phases. The measured H−C1−C2−H torsion angles in crystalline glucose were 170° ± 5° for the β-anomer and 40° ± 15° for the α-anomer, in good agreement with reported crystal structures. In the solution phase we give a full analysis of an experiment in which the cross-correlation effects are isolated by the use of a heteronuclear multiple-quantum filter. We consider the influence of anisotropic rotational diffusion, chemical shift anisotropy, and proton−proton spin diffusion on the torsion angle estimate. We show that it is possible to determine the torsion angle and the rotational correlation time independently. The measured H−C1−C2−H torsion angles in solution differ slightly from the solid-state results: 159° ± 10° for the β-anomer and 57° ± 7° for the α-anomer. For methyl-α-D-[1,3-$^{13}C_2$]-glucose, the solid phase double-quantum heteronuclear local field experiment was applied for the first time to a HCCH moiety in which the carbons are not directly bonded. These techniques may be applied to other structural problems such as the determination of glycosidic linkage conformations and the conformation of sugar rings in nucleotides.

I. Introduction

Carbohydrates play an important role in many biological processes.[1,2] Examples include (i) polysaccharides, which form the structural elements in the cell walls of bacteria and plants; (ii) sugars, which are important for energy storage and are also one of the main components of nucleotides[3]; and (iii) glycoconjugates (combinations of carbohydrates with lipids and proteins), which are important in many processes including cellular recognition.[1,2]

Insight into the biological and physicochemical functions of complex carbohydrates at the molecular level requires a precise understanding of their primary and secondary structure. Diffraction methods are of limited utility for complex carbohydrates and glycoconjugates because they tend to be difficult to crystallize. Nuclear magnetic resonance (NMR) techniques do not require well-formed crystals and are particularly important for obtaining molecular structural information in these systems.

Solution NMR is particularly useful for systems of relatively low molecular mass (less than around 30 000−50 000 molecular mass units). Solid-state NMR, on the other hand, has no essential restriction to systems of a certain molecular size and is expected to become increasingly useful in the study of large biomolecules.

In the NMR of carbohydrates, molecular structural information is obtained from (1) chemical shifts,[4,5] (2) through-bond *J*-couplings,[4,6] (3) through-space dipolar couplings, as estimated by cross-relaxation measurements[4,7,8] and experiments in partially ordered media,[9,10] and (4) the relative orientations of the nuclear spin interaction tensors, which may be estimated from various types of correlation experiments in the solid state[11−23] and from cross-correlated relaxation effects in the solution state.[24−30]

† Physical Chemistry Division.
‡ Present address: Department of Chemistry & Biochemistry, University of California, Los Angeles, CA 90095-1569.
§ Present address: ABB Corporate Research, Västerås, S-72178 Sweden.
|| Department of Organic Chemistry.
* Author for correspondence (E-mail: mhl@physc.su.se; phone: +46-8-162373; fax: +46-8-152187).

(1) *Glycosciences*; Gabius, H. J., Gabius, S., Eds.; Chapman & Hall: London, 1997.
(2) Ashwell, G.; Harford, J. *Annu. Rev. Biochem.* **1982**, *51*, 531.
(3) Saenger, W. *Principles of Nucleic Acid Structure*; Springer-Verlag: New York, 1984.
(4) van Halbeek, H. In *Encyclopedia of NMR*; Grant, D. M., Harris, R. K., Eds.; Wiley: New York, 1996; Vol. 2, p 1107.
(5) Zhang, P.; Klymachyov, A. N.; Brown, S.; Ellington, J. G.; Grandinetti, P. J. *Solid State Nucl. Magn. Reson.* **1998**, *12*, 221.
(6) Karplus, M. *J. Am. Chem. Soc.* **1963**, *85*, 2870.
(7) Mäler, L.; Kowalewski, J. *Chem. Phys. Lett.* **1992**, *190*, 241.
(8) Kovacs, H.; Bagley, S.; Kowalewski, J. *J. Magn. Reson.* **1989**, *85*, 530.
(9) Tjandra, N.; Bax, A. *Science* **1997**, *278*, 1111.
(10) Rundlöf, T.; Landersjö, C.; Lycknert, K.; Maliniak, A.; Widmalm, G. *Magn. Reson. Chem.* **1998**, *36*, 773.
(11) Weliky, D. P.; Tycko, R. *J. Am. Chem. Soc.* **1996**, *118*, 8487.
(12) Schmidt-Rohr, K. *J. Am. Chem. Soc.* **1996**, *118*, 7601.
(13) McDermott, A. E.; Creuzet, F.; Gebhard, R.; van der Hoef, K.; Levitt, M. H.; Herzfeld, J.; Lugtenburg, J.; Griffin, R. G. *Biochemistry* **1994**, *33*, 6129.
(14) Ishii, Y.; Terao, K.; Kainosho, M. *Chem. Phys. Lett.* **1996**, *256*, 133.
(15) Feng, X.; Lee, Y. K.; Sandström, D.; Edén, M.; Maisel, H.; Sebald, A.; Levitt, M. H. *Chem. Phys. Lett.* **1996**, *257*, 314.
(16) Feng, X.; Verdegem, P. J. E.; Lee, Y. K.; Sandström, D.; Edén, M.; Bovee-Geurts, P.; de Grip, W. J.; Lugtenburg, J.; de Groot, H. J. M.; Levitt, M. H. *J. Am. Chem. Soc.* **1997**, *119*, 6853.

10.1021/ja9910863 CCC: $19.00
Published on Web 01/26/2000

In this paper, we demonstrate the potential of the latter class of methods for studying carbohydrate conformations and configurations. In particular, we apply the method called HCCH double-quantum heteronuclear local field spectroscopy (HCCH-2Q-HLF),[15] which is suitable for $^{13}C_2$-labeled organic materials. The relative orientation of a pair of $^{13}C-^{1}H$ bond vectors is estimated through the evolution of the $^{13}C_2$ double-quantum coherence (2QC) under the proton local fields. This method has been applied to the measurement of H−C−C−H molecular torsion angles in solid samples of the membrane protein rhodopsin[16] and also an intermediate of the rhodopsin photocycle.[17] Other combinations of isotopes have also been used, allowing the estimation of N−C−C−N and H−C−N−H molecular torsion angles in solid peptides.[18−20] The 2Q-HLF technique has also been applied to solution NMR, where the heteronuclear local field correlations are manifested as differences in line widths of the double-quantum multiplet components.[24−26] In both solid-state and solution NMR, the evolution of the 2QCs under correlated heteronuclear dipolar interactions has been shown to provide accurate estimates of molecular torsion angles.

In this paper, we apply HCCH-2Q-HLF spectroscopy to two $^{13}C_2$-labeled carbohydrate samples, [1,2-$^{13}C_2$]-glucose and methyl-α-D-[1,3-$^{13}C_2$]-glucose (Figure 1). The former is a relatively "easy" system, in which the two ^{13}C nuclei are directly bonded, making it possible to excite $^{13}C_2$ 2QC with reasonable efficiency in both solids and liquids. The H−C1−C2−H torsion angle in crystalline [1,2-$^{13}C_2$]-glucose is estimated for both the α- and β-anomeric forms in both crystalline and solution phases. In the crystalline state we obtain results which are in good agreement with diffraction data. In viscous solution, the measured H−C1−C2−H torsion angle differs from the solid-state results by around 10°, which may reflect increased molecular flexibility or the influence of hydrogen bonding.

In solution we give a quantitative analysis of the experimental results incorporating anisotropic tumbling of the glucose molecules, chemical shift anisotropy, long-range heteronuclear dipolar interactions, and proton cross-relaxation.[25] We give a quantitative analysis of the heteronuclear multiple-quantum-filtered cross-relaxation trajectories, rather than employing the ratios of 2D peak amplitudes, as favored by other groups[24,26−30]. The use of full trajectories allows an independent estimate of the rotational correlation times, a quantitative comparison with spin−lattice relaxation rate constants (T_1), and a more detailed analysis of the importance of minor effects. For [1,2-$^{13}C_2$]-glucose, the effect of anisotropic molecuar tumbling is found to be minor.

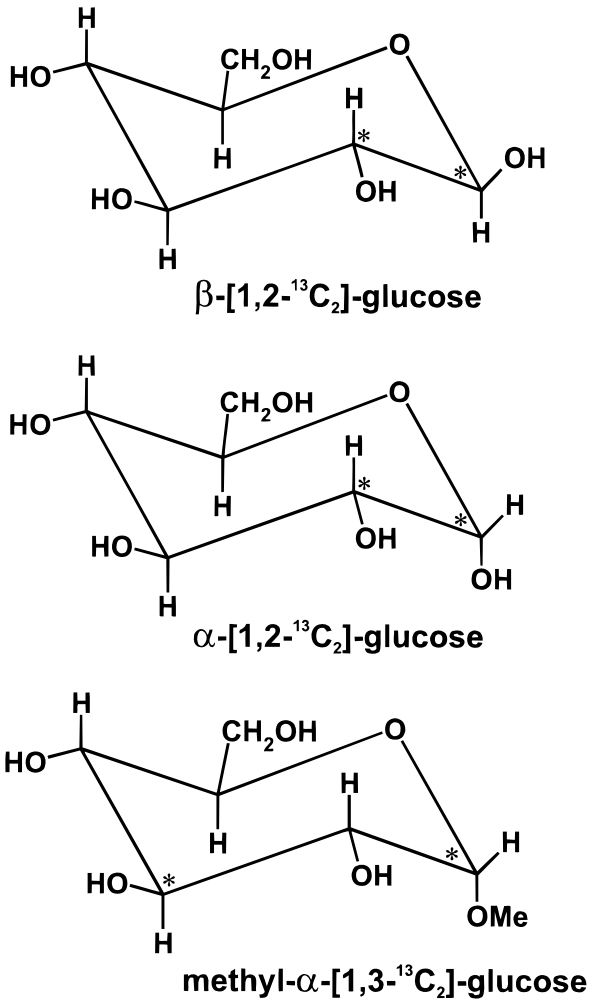

Figure 1. Structures of the anomers of [1,2-$^{13}C_2$]-glucose and methyl-α-D-[1,3−$^{13}C_2$]-glucose. The ^{13}C-labeled sites are indicated by asterisks.

The methyl-α-D-[1,3-$^{13}C_2$]-glucose sample is especially challenging because the ^{13}C nuclei are separated by two chemical bonds. It is difficult to apply the solution state version of the HCCH-2Q-HLF experiment in this case, because the $^{13}C-^{13}C$ *J*-coupling is negligible. Nevertheless, the solid-state version of the experiment proved to be feasible, and we could analyze the results quantitatively in terms of the geometrical relationship of the two $^{13}C-^{1}H$ bond vectors. To our knowledge, this is the first time that the solid-state HCCH-2Q-HLF experiment has been applied to a system with nonbonded $^{13}C_2$ pairs. These results prove the potential of 2Q-HLF techniques for obtaining geometrical information across the glycosidic linkage in polysaccharides, in which the carbon sites on neighboring sugar rings are also separated by two chemical bonds.

The results demonstrate that HCCH-2Q-HLF spectroscopy may be applied to complex carbohydrates, nucleic acids, or glycoproteins which are difficult to crystallize and in which the chemical shifts or *J*-couplings are difficult to exploit because of limited spectral resolution.

II. Nuclear Spin Interactions

1. Structural Parameters and Reference Frames. Most of the experiments described in this paper can be treated in terms

(17) Feng, X.; Verdegem, P. J. E.; Edén, M.; Sandström, D.; Lee, Y. K.; Bovee-Geurts, P.; de Grip, W. J.; Lugtenburg, J.; de Groot, H. J. M.; Levitt, M. H. *J. Biomol. NMR*, accepted for publication.

(18) Feng, X.; Edén, M.; Brinkmann, A.; Luthman, H.; Eriksson, L.; Gräslund, A.; Antzutkin, O. N.; Levitt, M. H. *J. Am. Chem Soc.* **1997**, *119*, 12006.

(19) Costa, P. R.; Gross, J. D.; Hong, M.; Griffin, R. G. *Chem. Phys. Lett.* **1997**, *280*, 95.

(20) Hong, M.; Gross, J. D.; Griffin, R. G. *J. Phys. Chem.* **1997**, *101*, 5869.

(21) Welicky, D. P.; Dabbagh, G.; Tycko, R. *J. Magn. Reson.* **1993**, *A104*, 10.

(22) Schmidt-Rohr, K. *J. Am. Chem. Soc.* **1996**, *118*, 7601.

(23) Gregory, D. M.; Mehta, M. A.; Shiels, J. C.; Drobny, G. *J. Chem. Phys.* **1997**, *107*, 28.

(24) Reif, B.; Hennig, M.; Griesinger, C. *Science* **1997**, *276*, 1230.

(25) Ravindranathan, S.; Feng, X.; Widmalm, G.; Levitt, M. H. 39th Experimental NMR Conference, Asilomar, CA, March 1998; poster 165.

(26) Griesinger, C.; Hennig, M.; Marino, J. P.; Reif, B.; Ritcher, C.; Schwalbe, H. In *Biological Magnetic Resonance*; Berliner, L. J., Ed.; Plenum Press: New York, 1999; Vol. 16, 259.

(27) Felli, I. C.; Ritcher, C.; Griesinger, C.; Schwalbe, H. *J. Am. Chem. Soc.* **1999**, *121*, 1956.

(28) Yang, D.; Konrat, R.; Kay, L. E. *J. Am. Chem. Soc.* **1997**, *119*, 1938.

(29) Reif, B.; Steinhagen, H.; Junker, B.; Reggelin, M.; Griesinger, C. *Angew. Chem., Int. Ed. Engl.* **1998**, *37*, 1903.

(30) Pelupessy, P.; Chiarparin, E.; Bodenhausen, G. *J. Biomol. NMR* **1999**, *14*, 277.

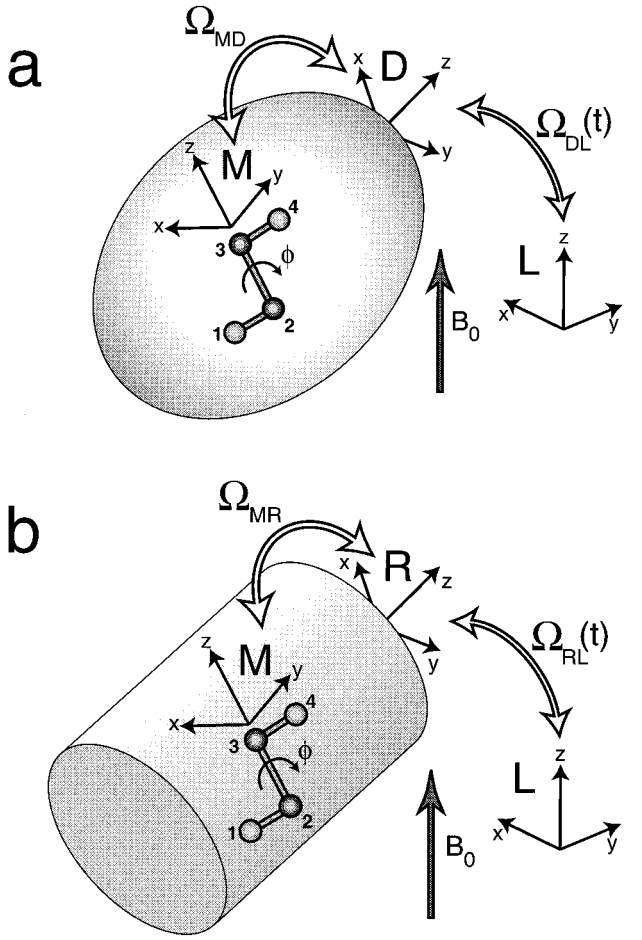

Figure 2. The relationship between the different reference frames for (a) a H−C−C−H unit in a molecule undergoing anisotropic rotational diffusion and (b) a H−C−C−H unit in a molecule undergoing magic-angle rotation in the solid state. In solution, the principal axis system of the diffusion tensor *D* is used as an intermediate reference frame. In magic-angle spinning solids, the rotor-fixed axis system *R* is used as an intermediate reference frame.

of a four-spin-1/2 model comprising the two ^{13}C spins (denoted as S_2 and S_3) and the two directly bonded protons (denoted I_1 and I_4), where I_1 is directly bonded to S_2 and I_4 is directly bonded to S_3 (Figure 2). The geometry of the four-spin unit is defined by several geometrical parameters, including the internuclear distances r_{12}, r_{23}, r_{34}; the two HCC bond angles θ_{123} and θ_{234}; and the H−C−C−H torsional angle denoted by ϕ. The four-spin unit is assumed to be rigid. A molecular reference frame *M* is defined so that its *z*-axis is along the S_2-S_3 internuclear vector. The positions of all four nuclei in the four-spin unit are considered fixed with respect to *M*.

Consider a fixed laboratory frame *L* which is defined such that the *z*-axis is parallel to the external static magnetic field B_0. In both liquids and rotating solids, the relationship between frames *M* and *L* is defined by three Euler angles $\Omega_{ML} = \{\alpha_{ML},\beta_{ML},\gamma_{ML}\}$, which are all time-dependent. In liquids this is because of random thermal molecular tumbling; in rotating solids, the time dependence is due to the mechanical motion.

In both phases of matter it is convenient to describe this time dependence in terms of an intermediate reference frame. In liquids, a suitable reference frame is the principal axis system of the rotational diffusion tensor, denoted *D* (Figure 2a). If the molecules are rigid, the relationship between frames *M* and *D* is defined by three fixed Euler angles $\Omega_{MD} = \{\alpha_{MD},\beta_{MD},\gamma_{MD}\}$. The Euler angles $\Omega_{DL} = \{\alpha_{DL},\beta_{DL},\gamma_{DL}\}$ defining the relationship of frames *D* and *L* are randomly time-dependent in a liquid. The correlation functions of these angles are given below for the case of anisotropic rotational diffusion.

In a rotating solid, it is more convenient to use an intermediate reference frame *R* for which the *z*-axis is parallel to the sample rotation axis (Figure 2b). The Euler angles $\Omega_{MR} = \{\alpha_{MR},\beta_{MR},\gamma_{MR}\}$ are random variables in a rotating powder, but are fixed for each molecule, assuming that the sample is well-packed and the molecules are rigid. The Euler angles $\Omega_{RL}(t) = \{\alpha_{RL}(t), \beta_{RL},\gamma_{RL}\}$ describe the macroscopic rotation of the sample. The angle $\alpha_{RL}(t)$ is given by $\alpha^0_{RL} - \omega_r t$, where α^0_{RL} is a stochastic variable (in nonrotor synchronized experiments), and ω_r is the angular rotation frequency. The angle β_{RL} defines the angle between the spinning axis and the magnetic field. In magic angle spinning experiments it is given by $\beta_{RL} = \tan^{-1} 2^{1/2}$. The Euler angle γ_{RL} is arbitrary.

2. Spin Hamiltonian. The spin Hamiltonian for the four-spin system is a sum of terms acting on the *I*-spins alone, the *S*-spins alone, and the interactions between the *I*-spins and the *S*-spins:

$$H(t) = H_I(t) + H_S(t) + H_{IS}(t) \tag{1}$$

The heteronuclear term involves a superposition of all four heteronuclear coupling terms:

$$H_{IS} = H_{12} + H_{13} + H_{24} + H_{34} \tag{2}$$

The high field truncated terms of these interactions are sufficient for the treatment of magic-angle spinning (MAS) NMR in high magnetic field and also for the treatment of transverse relaxation in the slow motion limit. The secular heteronuclear interactions are given by

$$H_{jk} = \omega_{jk} 2 I_{jz} S_{kz} \tag{3}$$

with

$$\omega_{jk} = \pi J_{jk} + \sum_{m=-2}^{2} b_{jk} D^2_{0m}(\Omega^{jk}_{PM}) D^2_{m0}(\Omega_{ML}) \tag{4}$$

assuming that the index *j* refers to an *I*-spin and index *k* refers to an *S*-spin. Here, I_{jz} and S_{kz} are spin operators, J_{jk} is the indirect *J*-coupling, and Ω^{jk}_{PM} represents the three Euler angles $\{\alpha^{jk}_{PM}, \beta^{jk}_{PM},\gamma^{jk}_{PM}\}$ relating the principal axis frame of the through-space interaction between I_j and S_k with the molecular frame *M*. For rigid systems, the through-space dipole−dipole coupling is given by

$$b_{jk} = -\frac{\mu_0}{4\pi}\frac{\gamma_j \gamma_k \hbar}{(r_{jk})^3} \tag{5}$$

where r_{jk} is the internuclear distance.

In the present paper, we exploit the geometrical content of b_{jk} and Ω^{jk}_{PM} to access the molecular geometrical information. The Euler angles Ω^{jk}_{PM} are related to the geometrical parameters of the four-spin system through

$$\beta^{12}_{PM} = \theta_{123} \tag{6}$$

$$\beta^{34}_{PM} = \pi - \theta_{234} \tag{7}$$

$$\gamma^{12}_{PM} - \gamma^{34}_{PM} = \gamma^{13}_{PM} - \gamma^{24}_{PM} = \phi \tag{8}$$

The Euler angles α^{12}_{PM}, etc., are arbitrary.

The Hamiltonian H_S contains the one-spin interactions of the S-spins

$$H_S = H_2 + H_3 \tag{9}$$

which may be written in general as

$$H_j = \omega_j S_{jz} \tag{10}$$

The frequency ω_j is given in terms of the chemical shift anisotropy (CSA) parameters of spin S_j, through

$$\omega_j = \omega_j^{\text{iso}} + \omega_j^{\text{aniso}} \sum_{m=-2}^{m} [D^2_{0m}(\Omega^j_{PM}) - \eta^j 6^{-1/2}(D^2_{2m}(\Omega^j_{PM}) + D^2_{-2m}(\Omega^j_{PM}))]\, D^2_{m0}(\Omega_{ML}) \tag{11}$$

where ω_j^{iso} and ω_j^{aniso} are the isotropic and anisotropic chemical shift frequencies, η^j is the asymmetry parameter, and Ω^j_{PM} is a Euler angle triplet defining the orientation of the CSA principal axis with respect to the frame M. The anisotropic chemical shift frequency is defined as $\omega_j^{\text{aniso}} = -\gamma_j B_0 \delta_j^{\text{aniso}}$, where δ_j^{aniso} is the CSA in ppm (deshielding convention), and B_0 is the magnetic field.

In this paper, the experiments are designed to be insensitive to the CSA parameters. However, several papers have shown that correlations in the CSA interactions may also be exploited to derive molecular geometrical information.[21−23,28]

3. Cross-Correlated Double-Quantum Evolution. The heteronuclear coupling terms such as H_{12} and H_{34}, are time-dependent in a rotating solid and for a tumbling molecule in a liquid, because in both cases the molecular orientational angles Ω_{ML} change with time. The modulations of the two different interactions (for example, H_{12} and H_{34}) are in general correlated because the relevant atoms are locked in a rigid molecular framework, with a definite geometry. The correlation of the spin interactions may be studied by utilizing the dynamics of the correlated nuclear spin state called 2QC. This was first demonstrated for the case of paramagnetic relaxation by Wokaun and Ernst.[31]

For a solid the rotation of the molecules is coherent, because all molecules are fixed with respect to a rigid crystalline lattice, which is subject to macroscopic rotation about a fixed axis at a fixed frequency. The 2QCs experience "coherent" cross-correlation effects, which can be studied in order to obtain geometrical information.[15−20] In a liquid on the other hand, the motion of the molecules is "incoherent". The 2QCs experience incoherent cross-correlated relaxation. This cross-correlated relaxation can also be analyzed to obtain useful information on the molecular geometry.[24−30] However, a quantitative treatment of the cross-correlated relaxation requires many assumptions as to the nature of the random molecular motion. In this paper, the cross-correlated relaxation in a viscous solution of [1,2-$^{13}C_2$]-glucose is studied in detail.

Although the solid-state and solution-state heteronuclear multiple-quantum local field experiments appear superficially to be quite different, they are in fact motivated by the same basic physics, as emphasized in Figure 2. In a Liouville space representation,[32] both experiments are conveniently analyzed by introducing the 2QC operators:

$$|\alpha + +\alpha) = |I_1^\alpha S_2^+ S_3^+ I_4^\alpha); \qquad |\alpha - -\alpha) = |I_1^\alpha S_2^- S_3^- I_4^\alpha)$$
$$|\alpha + +\beta) = |I_1^\alpha S_2^+ S_3^+ I_4^\beta); \qquad |\alpha - -\beta) = |I_1^\alpha S_2^- S_3^- I_4^\beta)$$
$$|\beta + +\alpha) = |I_1^\beta S_2^+ S_3^+ I_4^\alpha); \qquad |\beta - -\alpha) = |I_1^\beta S_2^- S_3^- I_4^\alpha)$$
$$|\beta + +\beta) = |I_1^\beta S_2^+ S_3^+ I_4^\beta); \qquad |\beta - -\beta) = |I_1^\beta S_2^- S_3^- I_4^\beta)$$

where the I spin projection operators are defined as

$$I_j^\alpha = \frac{1}{2} + I_{jz} \tag{12}$$

$$I_j^\beta = \frac{1}{2} + I_{jz} \tag{13}$$

These coherence operators are eigenoperators under commutation with the high-field spin Hamiltonian:

$$\hat{H}^{\text{comm}} |m_1 + +m_4) = -\omega_{m_1 m_4} |m_1 + +m_4) \tag{14}$$

$$\hat{H}^{\text{comm}} |m_1 - -m_4) = \omega_{m_1 m_4} |m_1 - -m_4) \tag{15}$$

where

$$\omega_{m1m4} = (\omega_2 + \omega_3) + m_1(\omega_{12} + \omega_{13}) + m_4(\omega_{24} + \omega_{34}) \tag{16}$$

The commutation superoperator is defined[32] $\hat{A}_{\text{comm}}|Q) = |[A,Q])$. All terms in eq 16 are time-dependent. The cross-correlations of the different terms are geometry sensitive, which allows the double-quantum evolution to probe the molecular geometry.

III. HCCH-2Q-HLF in Solids

In solids, it is possible to exploit the coherent evolution of 2QCs under the correlated heteronuclear local fields. To allow the ^{13}C spins to obtain a clear picture of the heteronuclear fields emanating from the protons, it is necessary to supress the $^1H-^1H$ interactions. This requires the use of a $^1H-^1H$ homonuclear decoupling pulse sequence during the 2Q evolution interval. This scales down the heteronuclear interactions as well as suppressing the homonuclear interactions. It is necessary to introduce a scaling factor κ for the heteronuclear couplings as a fit parameter in the analysis of the experimental results.

1. Pulse Sequence. The evolution of the 2QC under correlated heteronuclear dipolar interactions is monitored by the 2Q-HLF experiment,[15] employing the pulse sequence shown in Figure 3. The z-magnetization of the 1,2-$^{13}C_2$ pair is converted into 2QC by the C7 pulse scheme.[33] Other 2Q excitation schemes are also feasible[23,34,35]. The 2QC are allowed to evolve during the period τ_r, which is divided into two parts. The first part is a variable interval t_1 during which the homonuclear decoupling sequence MREV8 is applied. Other homonuclear decoupling pulse sequences may also be used.[36] The second part, $\tau_r - t_1$, is occupied by unmodulated high-power proton decoupling under which heteronuclear couplings are suppressed. A series of experiments are performed in which t_1 is incremented and τ_r

(31) Wokaun, A.; Ernst, R. R. *Mol. Phys.* **1978**, *36*, 317.
(32) Jeener, J. *Adv. Magn. Reson.* **1982**, *10*, 1.
(33) Lee, Y. K.; Kurur, N. D.; Helmle, M.; Johannessen, O. G.; Nielsen, N. C.; Levitt, M. H. *Chem. Phys. Lett.* **1995**, *242*, 304.
(34) Tycko, R.; Dabbagh, G. *J. Am. Chem. Soc.* **1991**, *113*, 9444.
(35) Sun, B. Q.; Costa, P. R.; Kocisko, D.; Lansbury, P. T.; Griffin, R. G. *J. Chem. Phys.* **1995**, *102*, 702.
(36) Bielecki, A.; Kolbert, A. C.; de Groot, H. J. M.; Griffin, R. G.; Levitt, M. H. *Adv. Magn. Reson.* **1989**, *14*, 111.

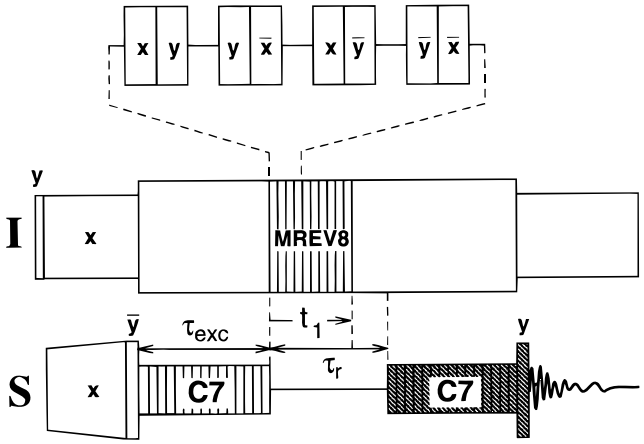

Figure 3. Pulse sequence for the solid-state HCCH-2Q-HLF experiment.

$-\ t_1$ contracted so that the total interval remains equal to one rotor period. This removes the effect of ^{13}C shift anisotropies on the 2QC evolution. The effect of isotropic chemical shifts is removed by a suitable choice of the spectrometer reference frequency. The modulated 2QCs are converted to z-magnetization by a second C7 sequence and a further $\pi/2$ pulse leads to observable signal.

2. [1,2-$^{13}C_2$]-Glucose. Figure 4 shows the ^{13}C cross-polarization (CP)/MAS spectrum and the double-quantum filtered spectrum of crystalline [1,2-$^{13}C_2$]-glucose. Signals are observed for both α- and β-anomers. The smaller peaks are assigned to the β-anomer and the larger peaks to the α-anomer. This is consistent with the isotropic chemical shift difference of about 4 ppm.[37] Comparison of the two spectra show that the ^{13}C signals are passed through 2QC with about 37% efficiency. It was difficult to optimize the pulse sequence to obtain higher efficiency, because the proton relaxation time constant was long ($\approx$ 20 s).

The theoretical expression for the signal in the 2Q-HLF experiment is[15]

$$f(t_1) = \left\langle \frac{1}{2}\{\cos\Phi^{\alpha\alpha}(t_1) + \cos\Phi^{\alpha\beta}(t_1)\}\sin^2(\omega_{2Q}\tau_{exc})\right\rangle_{av} \qquad (17)$$

The brackets indicate averaging over all molecular orientations Ω_{MR}. ω_{2Q} denotes the orientation-independent double-quantum nutation frequency during the C7 sequences. For C7, ω_{2Q} depends on the orientation only through the Euler angle β_{MR}.[33] The phase angles $\Phi^{\alpha\alpha}$ and $\Phi^{\alpha\beta}$ correspond to the coherent evolution phases of the $|\alpha - -\alpha)$ and $|\alpha - -\beta)$ 2Q coherences:

$$\Phi^{m_1 m_4}(t) = 2\kappa\int_0^{t_1}\{m_1[\omega_{12}(t) + \omega_{13}(t)] + m_4[\omega_{42}(t) + \omega_{43}(t)]\}\,dt \qquad (18)$$

where m_1 and m_4 are the quantum numbers for the proton spin states. The heteronuclear dipolar interaction frequencies ω_{jk} are given by eq 4. The torsion angle is determined by fitting theoretical curves of the form

$$\alpha(t_1) = Af(t_1,\kappa,\phi)e^{-\lambda t_1} \qquad (19)$$

to the experimental signal amplitudes. The factor A sets the experimental vertical scale. f is given by eq 17 and is dependent on the evolution time, the multiple pulse scaling factor, the torsion angle, and the other geometrical parameters of the four-spin system. The decay in signal amplitudes due to $^1H-^1H$ spin diffusion under the evolution interval t_1 is taken into account by a phenomenological damping constant λ. In general A, λ, and κ are treated as empirical fit parameters.

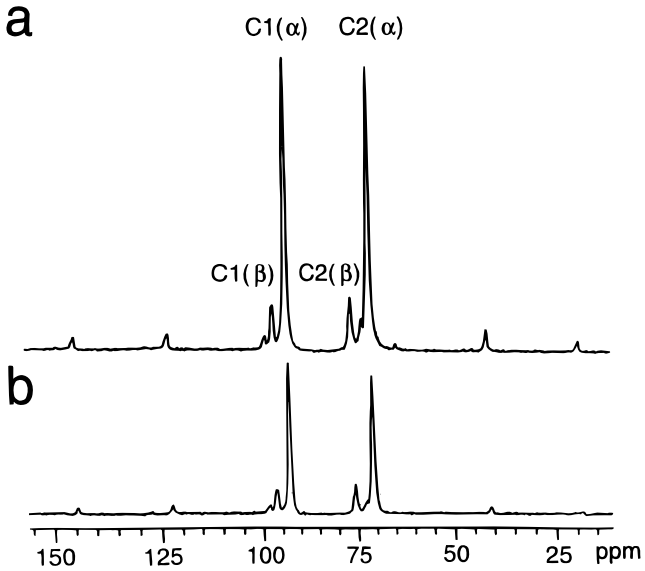

Figure 4. (a) Cross-polarization magic-angle spinning spectrum of crystalline [1,2-$^{13}C_2$]-glucose. (b) Spectrum obtained by ^{13}C double-quantum filtration using the C7 pulse sequence. Assignments are from ref 37.

In the simulations shown below, the following molecular structural parameters were used: $r_{12} = r_{34} = 0.113$ nm, $\theta_{123} = 115.3°$, and $\theta_{234} = 108.7°$. These parameters correspond to diffraction measurements on crystalline β-glucose,[38] with the exception of the direct C−H bond lengths, where neutron diffraction measurements on α-glucose indicate a distance of 0.1114 nm.[39] The effective bond length as measured by NMR is influenced by vibrational motion. Corrections based on the combined effect of harmonic and anharmonic stretching and vibrational rocking, increases the effective value to 0.113 nm.[40,41]

Figure 5a shows experimental double-quantum signal trajectories for the β-anomer. The experimental amplitudes are obtained by integration of the signals from the two peaks. The figure also shows the simulated curves for several different torsional angles. In each case, the parameters A and λ are optimized in order to minimize the deviations of simulations and experimental points. For the β-anomer the best fit to the experimental data is obtained for a torsion angle of 170°. The simulation for a torsion angle of 180° gives a slightly poorer fit, and the simulation for 160° deviates significantly from the experimental points. All simulated curves employ a heteronuclear scaling factor of $\kappa = 0.45$, which is a reasonable value for the semiwindowless MREV8.

The high sensitivity of the simulations to the torsion angle in the region of ϕ close to 180° has a physical interpretation. If the geometry corresponds to $\phi = 180°$, the one-bond C−H couplings are parallel and the heteronuclear dipolar fields exactly cancel out for the $|\alpha - -\beta)$, $|\beta - -\alpha)$, $|\alpha + +\beta)$, and $|\beta + +\alpha)$ coherences. This implies that four out of the eight 2QCs are completely unmodulated by the strong magnetic fields emanating from the neighboring protons. The phase angles

(37) Pfeffer, P. E.; Hicks, K. B.; Frey, M. H.; Opella, S. J.; Earl, W. L. *J. Carbohydr. Chem.* **1984**, *3*, 197.
(38) Chu, S. S. C.; Jeffrey, G. A. *Acta Crystallogr.* **1968**, *B24*, 830.
(39) Brown, G. M.; Levy, H. A. *Acta Crystallogr.* **1979**, *B35*, 656.
(40) Nakai, T.; Ashida, J.; Terao, T. *Mol. Phys.* **1989**, *67*, 839.
(41) Ishii, Y.; Terao, T.; Hayashi, S. *J. Chem. Phys.* **1997**, *107*, 2760.

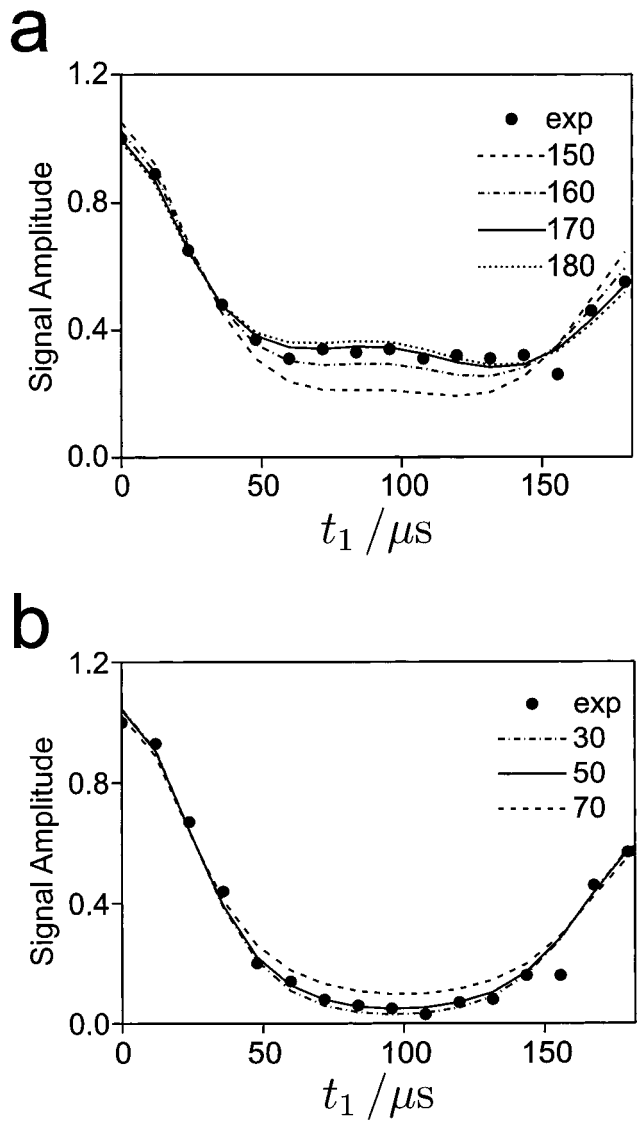

Figure 5. Signal amplitudes for the β-anomer (a) and α-anomer (b) of crystalline [1,2-$^{13}C_2$]-glucose in a double-quantum heteronuclear local field experiment. The symbols indicate experimental integrated signal amplitudes as a function of the evolution interval t_1. The lines are best fit simulations for different torsion angles, optimizing the damping factor and vertical scale independently for each curve.

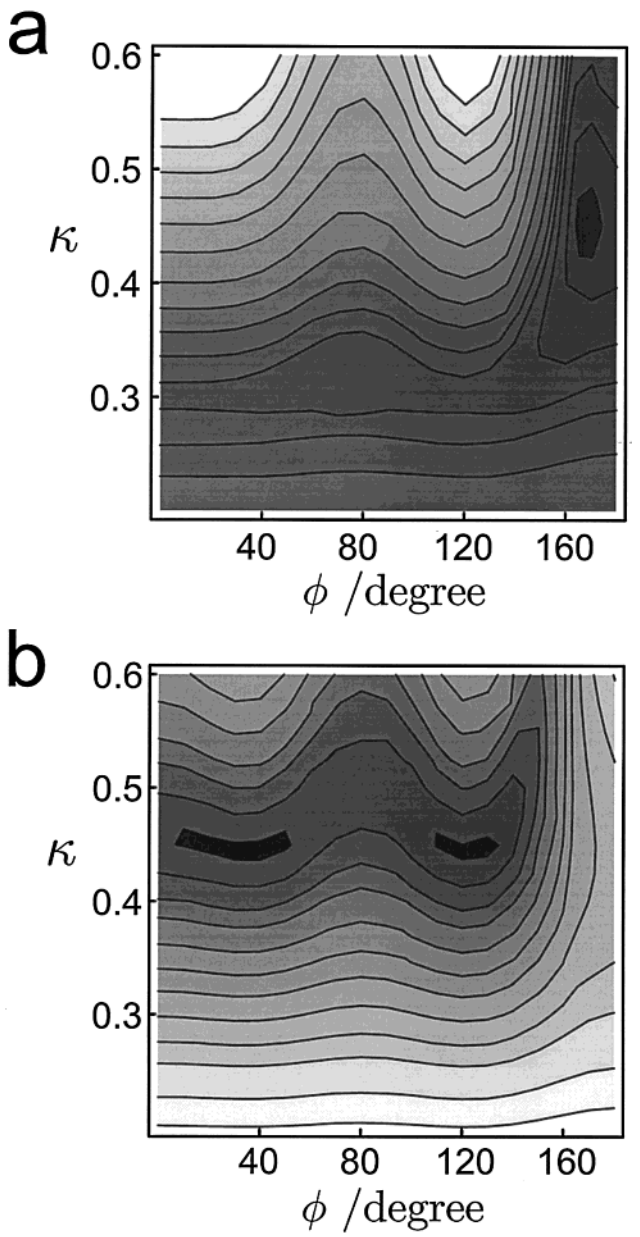

Figure 6. Surface showing the mean square deviation between experimental and simulated signal amplitudes for (a) β-[1,2-$^{13}C_2$]-glucose and (b) α-[1,2-$^{13}C_2$]-glucose. The mean square deviation is plotted as a function of the multiple pulse scaling factor κ and the H−C1−C2−H torsion angle. Dark regions represent minima.

$\Phi^{\alpha\beta}(t_1)$ and $\Phi^{\beta\alpha}(t_1)$ in eq 18 are exactly zero for all t_1 values in this geometrical configuration. This delicate balance is disturbed as soon as ϕ deviates significantly from 180°. The most sensitive region is close to 180°, where the balance of heteronuclear local fields is only slightly broken.

Figure 5b shows the corresponding results for the α-anomer. The best fit is obtained for $\phi = 50°$. In this case, the torsion angle resolution is lower and it is barely possible to distinguish the best fit simulation for $\phi = 50°$ from the simulation with $\phi = 30°$. However, the simulation with $\phi = 70°$ is clearly in disagreement.

To study the effect of the scaling factor κ, we carried out simulations for different values of κ spanning the entire torsion angle space. In Figure 6 we show contour plots representing the mean square deviation between the simulated curves and experimental data. The κ value corresponding to the minimum is well-defined for the entire torsion angle range and is 0.45 for both anomers. This implies that the torsion angle can be estimated without an independent determination of the scaling factor κ.

These contour plots indicate that the determination of ϕ is precise in the region close to 180°, which is the case for the β-anomer (Figure 6a). In this region of ϕ a torsional angle resolution of ±5° can be claimed. The torsion angle is unambiguous in this region if one discounts the sign of ϕ, which cannot be determined. The resolution is much lower in the case of the α-anomer (Figure 6b). Furthermore, there is a second minimum around $\phi = 120°$, making the torsion angle determination in this region of ϕ ambiguous. Nevertheless, the experiment may still be useful for ruling out some qualitative structural models.

Note that the values chosen for the one-bond internuclear distances r_{12}, r_{23}, and r_{34} are of little consequence for the determination of ϕ. Within a broad range, the simulations are only sensitive to the products κr_{12}^{-3} and κr_{34}^{-3}, because the spin dynamics are dominated by the nearest neighbor interactions between each ^{13}C and its directly bonded proton. If a different

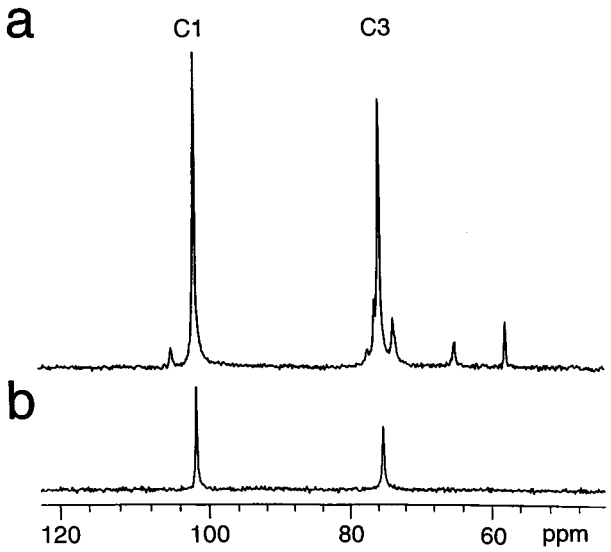

Figure 7. (a) Cross-polarization magic-angle spinning spectrum of methyl-α-D-[1,3−$^{13}C_2$]-glucose diluted in unlabeled material. The weaker peaks are from natural ^{13}C spins. (b) Spectrum obtained by $^{13}C_2$ double-quantum filtration using the C7 sequence. Assignments are from ref 54.

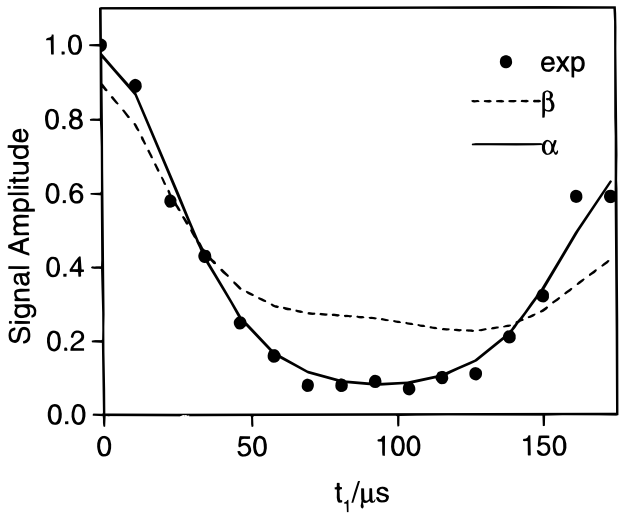

Figure 8. Signal amplitudes for methyl-α-D-[1,3−$^{13}C_2$]-glucose in a double-quantum heteronuclear local field experiment. The symbols indicate experimental integrated signal amplitudes as a function of the evolution interval t_1. The lines are best fit simulations for molecular geometries corresponding to the α- and β-anomer, optimizing the damping factor and vertical scale independently for each curve.

value is chosen for the one-bond C−H distance, the κ value required for the best fit changes but the determined torsion angle does not.

The best fit simulations for both the anomers agree well with the results from diffraction studies of crystalline glucose.[38,39] For the β-anomer the solid-state NMR determination is 170 ± 5°, which is in excellent agreement with the estimate from X-ray crystallography of $\phi = 171°$. For the α-anomer, solid-state NMR gives 40° ± 15° which is also in agreement with the neutron diffraction estimate of 50.6°. However, in this case the NMR determination of the torsion angle is not capable of high accuracy and is also ambiguous, as discussed above. Clearly, 2Q-HLF results should be combined with other experimental data, for example internuclear distance measurements, chemical shifts, or *J*-coupling information, to obtain reliable definition of the geometry in this region of ϕ.

3. Methyl-α-D-[1,3-$^{13}C_2$]-glucose. In this sample, the labeled sites are separated by two bonds and are at a distance of 0.249 nm. This makes it more difficult to achieve excitation of the $^{13}C_2$ 2QC. Solution state 2Q-HLF experiments are very difficult in this compound, due to the negligible $^2J_{CC}$ coupling constant ($^2J_{CC} \approx 0$ Hz).[42]

Figure 7a shows the ^{13}C CP/MAS spectrum of the sample of methyl-α-D-[1,3-$^{13}C_2$]-glucose (henceforth referred to as 1,3-mag). As described in the Experimental Section, the sample was diluted with unlabeled methyl-α-D-glucose in a molar ratio 1:10, to magnetically isolate the $^{13}C_2$ pairs. The CP/MAS spectrum shows two strong signals from the ^{13}C labels and also a number of smaller peaks from natural ^{13}C spins. The 2Q filtered spectrum is shown in Figure 7b and displays signals from the $^{13}C_2$ labels alone. The ^{13}C signals are passed through 2QC with 29% efficiency. Further optimization of 2Q excitation was impeded by the long ^1H relaxation time constant of around 10 s at room temperature.

Figure 8 shows the results of the 2Q-HLF experiment on 1,3-mag. The experimental points are plotted as a function of evolution interval t_1. Best fit simulations are also shown for the α and β configurations. These simulations employ spatial configurations of the four spins appropriate to the two different geometries, and in each case allow *A*, κ, and λ to vary in order to obtain the best fit with the experimental results. The best fit to the experimental points is clearly obtained for the α-anomer as expected. The best fit κ value for this case was 0.45. These results indicate that solid-state 2Q-HLF spectroscopy is capable of determining geometric relationships over a larger distance range than a single chemical bond. Indeed, the solution state HCCH-2Q-HLF experiment was conducted to obtain geometrical information over a distance of around 0.7 nm.[28] In the context of carbohydrates, the present results indicate the feasibility of examining conformations across the glycosidic linkage in oligosaccharides by solid-state HCCH-2Q-HLF spectroscopy. Preliminary results on a $^{13}C_2$-labeled disaccharide were obtained, and will be presented elsewhere.

IV. Cross-Correlated Double-Quantum Relaxation in Liquids

In liquids, the Euler angles $\Omega_{DL}(t)$ are randomly modulated, leading to cross-correlated incoherent relaxation of the 2QCs. Analysis of this cross-correlated relaxation allows determination of molecular geometry, providing suitable assumptions are made as to the anisotropy of the molecular tumbling. A range of experimental procedures were developed to minimize the effect of undesirable cross-correlation and cross-relaxation terms.[24,26,27] Typically, this involves taking the ratios of peak amplitudes at a single mixing interval. Such experiments have been applied to biological systems including proteins and RNA molecules in solution.[27]

In this section, the cross-correlated relaxation in a sample of [1,2-$^{13}C_2$]-glucose is studied in some detail.[25] To study the relaxation processes at long correlation times (which are usually relevant for biomolecules), we use a concentrated (1 M) solution of [1,2-$^{13}C_2$]-glucose in glycerol. The strong NMR signal of this sample also allows us to use a simplified experimental procedure in which the number of coherence transfer steps is minimized. We study the trajectory of the coherence transfer process in detail and investigate the importance of various minor effects on the transfer curves, in particular motional anisotropy and proton−proton cross-relaxation. We give a quantitative

(42) Walker, T. E.; London, R. E.; Wahley, T. W.; Barker, R.; Matwiyoff, N. A. *J. Am. Chem. Soc.* **1976**, *98*, 5807.

Table 1. Precession Frequencies and Relaxation Rate Constants of the Double-Quantum Coherences in a Four-Spin System

operator	frequency/rad s^{-1}	relaxation rate constant
$\|\alpha\,-\,-\alpha)$	$\omega_{\alpha\alpha} = \omega_2^{iso} + \omega_3^{iso} + \pi(J_{12} + J_{13} + J_{24} + J_{34})$	$R_{\alpha\alpha}$
$\|\alpha\,-\,-\beta)$	$\omega_{\alpha\beta} = \omega_2^{iso} + \omega_3^{iso} + \pi(J_{12} + J_{13} - J_{24} - J_{34})$	$R_{\alpha\beta}$
$\|\beta\,-\,-\alpha)$	$\omega_{\beta\alpha} = \omega_2^{iso} + \omega_3^{iso} + \pi(-J_{12} - J_{13} + J_{24} + J_{34})$	$R_{\beta\alpha}$
$\|\beta\,-\,-\beta)$	$\omega_{\beta\beta} = \omega_2^{iso} + \omega_3^{iso} + \pi(-J_{12} - J_{13} - J_{24} - J_{34})$	$R_{\beta\beta}$
$\|\alpha\,+\,+\alpha)$	$-\omega_{\alpha\alpha}$	$R_{\alpha\alpha}$
$\|\alpha\,+\,+\beta)$	$-\omega_{\alpha\beta}$	$R_{\alpha\beta}$
$\|\beta\,+\,+\alpha)$	$-\omega_{\beta\alpha}$	$R_{\beta\alpha}$
$\|\beta\,+\,+\beta)$	$-\omega_{\beta\beta}$	$R_{\beta\beta}$

description of the molecular geometry and the molecular tumbling, and compare the solution and solid-state geometries.

1. Multiple-Quantum Line Widths. In isotropic liquids, the spin Hamiltonian may be written

$$H = H^{iso} + H^{aniso}(t) \tag{20}$$

where H^{iso} is the isotropic part of the spin Hamiltonian (including isotropic chemical shifts and J-couplings). The behavior of the spin system is characterized by coherent evolution under the isotropic spin Hamiltonian, combined with relaxation under the incoherently modulated anisotropic part. If the random modulation is sufficiently fast (Redfield limit),[43] the spin density operator ρ evolves according to the Liouville von Neumann equation

$$\frac{d\rho}{dt} = -i[H^{iso},\rho] + \hat{\Gamma}\rho \tag{21}$$

where $\hat{\Gamma}$ is the relaxation superoperator.

The matrix elements of $\hat{\Gamma}$ are given by[44]

$$\Gamma_{rs} = (Q_r|\hat{\Gamma}|Q_s) \tag{22}$$

$$= \int_0^\infty d\tau (Q_r|[H^{aniso}(\tau),[H^{aniso}(0),Q_s]]) \tag{23}$$

where Q_r and Q_s are orthonormal operators, and the superoperator bracket is defined[32]

$$(Q_r|Q_s) = \mathrm{Tr}\{Q_r^\dagger Q_s\}\,\delta_{rs}$$

The experiments described in this paper exploit the relaxation of 2QC between the spins S_2 and S_3. The 2QCs are eigenoperators under commutation with the isotropic Hamiltonian H^{iso}, for example

$$(\hat{H}^{iso})^{comm}|\alpha\,-\,-\alpha) = \omega_{\alpha\alpha}|\alpha\,-\,-\alpha) \tag{25}$$

and the coherence frequencies $\omega_{\alpha\alpha}$ are given in Table 1.

If all the coherences of a particular order are well-resolved ($\omega_{\alpha\alpha} \neq \omega_{\alpha\beta} \neq \omega_{\beta\alpha} \neq \omega_{\beta\beta}$ in the case of 2Q evolution), then the cross-relaxation of coherences into each other may be neglected. Only the diagonal elements of the relaxation superoperator need be taken into account. The relevant matrix elements of the relaxation superoperator are

$$R_{\alpha\alpha} = -(\alpha\,-\,-\alpha|\hat{\Gamma}|\alpha\,-\,-\alpha) = (\alpha\,+\,+\alpha|\hat{\Gamma}|\alpha\,+\,+\alpha) \tag{26}$$

where $R_{\alpha\alpha}$ is the relaxation rate constant for the coherence $|\alpha\,-\,-\alpha)$.

If the molecules undergo anisotropic rotational diffusion, the stochastic variation of the angles Ω_{DL} leads to the following correlation function for the Wigner matrix elements:[45]

$$\langle D^L_{n,m}(\Omega_{DL}(0))D^L_{-n',m}(\Omega_{DL}(\tau))^*\rangle = \frac{1}{2L+1}\sum_{\nu=-L}^{L} c_{\nu n}^{(L)}\, c_{\nu -n'}^{(L)} \exp\{-b_\nu^{(L)}\tau\} \tag{27}$$

where $c_{\nu n}(L)$ are the eigenvectors and $b_\nu(L)$ are the eigenvalues of the rotational diffusion operator. For slow rotational tumbling in a liquid ($\omega_0^S\tau_c > 1$, where ω_0^S is the S-spin Larmor frequency and τ_c is the motional correlation time), the general form of the relaxation rate constants is

$$\begin{aligned} R_{m_1m_4} = {} & \frac{2}{3}\{J_{21,21} + J_{24,24} + J_{31,31} + J_{34,34}\} + \\ & \frac{8}{3}\{J_{2,2} + J_{3,3}\} + \\ & \frac{4}{3}\{J_{21,31} + J_{24,34} + 4m_1m_4(J_{24,21} + J_{34,31} + \\ & \qquad J_{24,31} + J_{21,34})\} - \\ & \frac{8}{3}\{2m_1(J_{21,2} + J_{21,3} + J_{31,2} + J_{31,3}) + 2m_4(J_{14,1} + \\ & \qquad J_{14,3} + J_{34,1} + J_{34,3})\} + \\ & \frac{16}{3}J_{2,3} + R^{nonad}_{m_1m_4} \end{aligned} \tag{28}$$

where m_1 and m_4 represent quantum numbers for the proton spin states and $R^{nonad}_{m_1m_4}$ takes into account nonadiabatic longitudinal cross-relaxation (see below). For example, the relaxation rate constant $R_{\alpha\beta}$ may be derived by inserting $m_1 = 1/2$ and $m_4 = -1/2$ in the equation above. The subscripts with two spin labels denote a dipolar interaction and subscripts with a single spin label denote a CSA interaction. For example, the term $J_{21,2}$ represents the spectral density for the cross-correlation of the dipole−dipole interactions between spins S_2 and I_1, and the chemical shift interaction of spin S_2, evaluated at frequency $\omega = 0$:

$$\begin{aligned} J_{21,2} = {} & \frac{1}{5}\left(\frac{\mu_0}{4\pi}\frac{\gamma_2\gamma_1\hbar}{r_{21}^3}\right)\delta_2^{aniso}\gamma_2 B_0 \times \\ & \sum_{\nu=-2}^{2}\sum_{nn'=-2}^{2}\sum_{pp'=-2}^{2} D^{(2)}_{0p}(\Omega^{21}_{PM})D^{(2)}_{pn}(\Omega_{MD}) \times \\ & \left\{D^{(2)}_{0p'}(\Omega^2_{PM}) - \frac{\eta_2}{6^{1/2}}[D^{(2)}_{2p'}(\Omega^2_{PM}) + D^{(2)}_{-2p'}(\Omega^2_{PM})]\right\} \times \\ & D^{(2)}_{p'n'}(\Omega_{MD})\frac{c^{(2)}_{\nu n}\, c^{(2)}_{\nu -n'}}{b^{(2)}_\nu} \end{aligned} \tag{29}$$

Here η_2 is the asymmetry parameter of the chemical shift anisotropy of site 2. The term $J_{21,31}$ represents the spectral density for the cross-correlation of the dipolar interaction pairs,

(43) Slichter, C. P. *Principles of Magnetic Resonance*; Springer: Berlin, 1989.

(44) Ernst, R. R.; Bodenhausen, G.; Wokaun, A. *Principles of Nuclear Magnetic Resonance in One and Two Dimensions*; Oxford: New York, 1987.

(45) Grant, D. M.; Brown, R. A. In *Encyclopedia of NMR*; Grant, D. M., Harris, R. K., Eds.; Wiley: New York, 1996; Vol. 6, p 4003.

S_2-I_1 and S_3-I_1, evaluated at frequency $\omega = 0$:

$$J_{21,31} = \frac{1}{5}\left(\frac{\mu_0}{4\pi}\frac{\gamma_2\gamma_1\hbar}{r_{21}^3}\right)\left(\frac{\mu_0}{4\pi}\frac{\gamma_3\gamma_1\hbar}{r_{31}^3}\right) \times \sum_{\nu=-2}^{2}\sum_{nn'=-2}^{2}\sum_{pp'=-2}^{2} D_{0p}^{(2)}(\Omega_{PM}^{21}) D_{pn}^{(2)}(\Omega_{MD}) \times D_{0p'}^{(2)}(\Omega_{PM}^{31}) D_{p'n'}^{(2)}(\Omega_{MD}) \frac{c_{\nu n}^{(2)}\, c_{\nu -n'}^{(2)}}{b_\nu^{(2)}} \quad (30)$$

Similar equations apply to the other spectral densities. The spectral densities depend in general on the molecular geometrical parameters (through the Euler angles Ω_{PM}^{j}, Ω_{PM}^{jk}) and also on the orientation of the principal axis system of the rotational diffusion tensor with respect to the molecular frame (through the Euler angles Ω_{MD}).

The case of isotropic rotational diffusion with correlation time τ_c may be treated by using $b_0^{(2)} = \tau_c^{-1}$ and $c_{\nu n}^{(2)} = \delta_{\nu 0}$, where $\delta_{\nu 0}$ is a Kronecker delta function.

The presence of cross-correlation results in different relaxation rate constants for the four lines of the 2Q spectrum ($R_{\alpha\alpha} \neq R_{\alpha\beta} \neq R_{\beta\alpha} \neq R_{\beta\beta}$). This is observed experimentally as differential line widths in the 2Q spectrum.[24−26]

For an accurate analysis of the relaxation, one must take into account the low-frequency nonadiabatic contributions ($R_{m_1 m_4}^{\text{nonad}}$ in eq 28). These terms correspond to the longitudinal cross-relaxation between the two protons in the four-spin unit, and also longitudinal cross-relaxation processes involving other protons in the same molecule. These processes are significant even in the case of slow molecular rotation, because they involve small differences in proton Zeeman energies. In the calculations given below we incorporate the following nonadiabatic corrections:

$$R_{\alpha\alpha}^{\text{nonad}} = R_{\beta\beta}^{\text{nonad}} = R_{\text{ext}} \quad (31)$$

$$R_{\alpha\beta}^{\text{nonad}} = R_{\beta\alpha}^{\text{nonad}} = \frac{1}{3}J_{14,14} + R_{\text{ext}} \quad (32)$$

where

$$R_{\text{ext}} = \frac{1}{3}\sum_{l\neq 1,4}(J_{1l,1l} + J_{4l,4l}) \quad (33)$$

The term $J_{14,14}$ takes into account the cross-relaxation between spins I_1 and I_4, whereas the term R_{ext} involves a sum of cross-relaxation probabilities between spin I_1 or spin I_4 and other protons I_l in the same molecule. Note that the cross-relaxation between spins I_1 and I_4 leads to differential line broadening of the double-quantum multiplet components, mimicking the cross-correlation effects. This term must therefore be investigated carefully.

Long-range J-couplings between the ^{13}C spins and distant ^{1}H nuclei in the same molecule also lead to broadening of the 2Q multiplet peaks. However, evolution under long-range J-couplings is suppressed in the experimental strategy chosen in this paper (see below).

2. Estimate of Rotational Correlation Times. The labeled glucose was dissolved in a viscous solvent (glycerol), so as to impede the rotational tumbling of the molecules. The rotational correlation time was estimated by measuring the spin−lattice relaxation time constants (T_1) for the ring carbons of unlabeled glucose, under identical conditions. The results were 0.67 ± 0.03 s for β-glucose and 0.60 ± 0.02 s for α-glucose, where the indicated variation indicates the spread of T_1 values for the different ^{13}C sites. These T_1 values correspond to rotational correlation times of $\tau_c = 9.5$ ns (for β-glucose) and $\tau_c = 8.4$ ns (for α-glucose), assuming that the rotational tumbling is isotropic and dominated by short-range heteronuclear dipolar interactions. Both correlation times satisfy $|\omega_0\tau_c| > 1$, where ω_0 is the ^{13}C Larmor frequency. This supports the validity of eq 28 under the conditions used here.

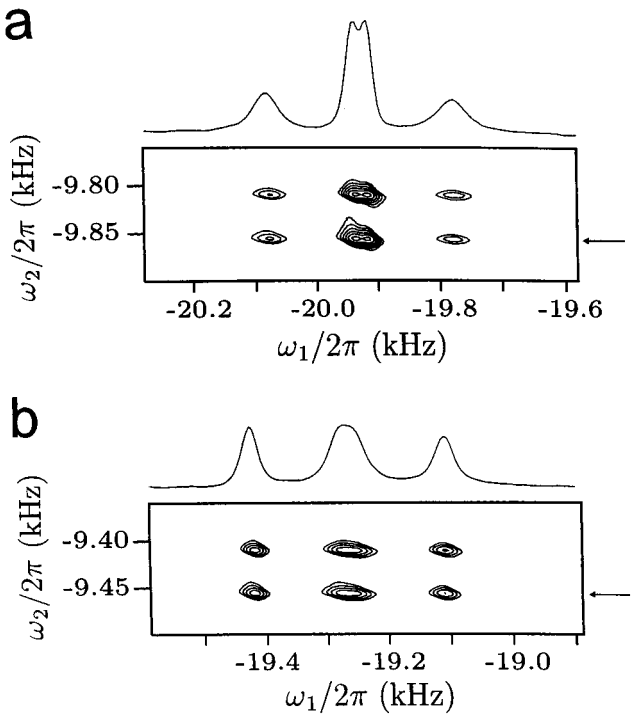

Figure 9. Sections of the 2D double-quantum ^{13}C spectrum of the $^{13}C_2$-glucose solution. (a) Contour plot of the spectral region containing signals from the C1 carbon of the β-anomer. (b) Contour plot of the spectral region containing signals from the C1 carbon of the α-anomer. The slices parallel to the ω_1 axis show the peaks corresponding to the four 2QCs. The slices are taken at the ω_2 coordinates indicated by arrows. The frequencies are specified relative to the Larmor frequency of the most shielded ^{13}C peak of glycerol. The signs of the frequencies are specified as in ref 60.

3. 2Q Spectrum of [1,2-$^{13}C_2$]-Glucose. Figure 9 shows two spectral regions of the 2Q ^{13}C spectrum of [1,2-$^{13}C_2$]-glucose, corresponding to the C1 signals of the β- and α-anomers. The C2 spectral regions have a similar appearance (not shown). The 2D spectrum was obtained using the standard 2D-INADEQUATE pulse sequence[46] (Figure 10a). The proton decoupling was turned off during the evolution period in order to resolve the four 2Q coherences. Figure 9 shows sections of the 2D spectrum, displaying signals from the β-anomer (Figure 9a) and the α-anomer (Figure 9b). Each slice parallel to the ω_1-axis contains four peaks, corresponding to the four 2QCs. The differential peak broadening in these multiplets is visually obvious.

4. Heteronuclear Multiple-Quantum Filtered 2Q Spectra. Several groups[24,26−30] have developed methods in which the cross-correlation effects are estimated through the ratios of peak amplitudes, after allowing the 2Q coherences to evolve over a constant time interval which is assumed to be small. This approach simplifies the analysis but tends to obscure the influence of minor perturbations of the cross-correlated relax-

(46) Bax, A.; Freeman, R.; Frenkiel, T.; Levitt, M. H. *J. Magn. Reson.* **1981**, *43*, 478.

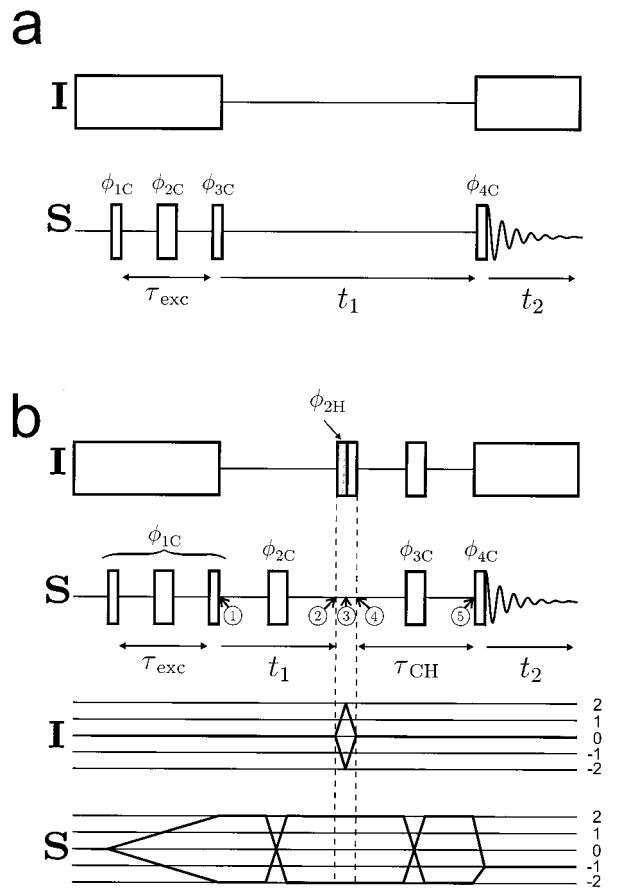

Figure 10. (a) Pulse sequence for the 2D double-quantum NMR experiment. WALTZ-16 ^{1}H decoupling is applied during 2QC excitation and signal acquisition. (b) Pulse sequence for the heteronuclear multiple-quantum-filtered experiment and corresponding coherence transfer pathway diagram. The narrow rectangles indicate $\pi/2$ pulses and the broad rectangles indicate π-pulses.

ation trajectories. In this paper, we describe the full trajectory of the cross-correlated double-quantum relaxation as a function of time, allowing a detailed study of the molecular dynamics and the geometry. The effects of dipole−dipole cross-correlation are isolated by using a heteronuclear multiple-quantum filter. The approach is similar to the multiple-quantum filtered nuclear Overhauser enhancement spectroscopy (NOESY) experiment which measures cross-correlation effects in longitudinal relaxation.[47−50] Similar approaches have been used for extracting cross-correlation effects in the relaxation of single-quantum coherences.[51,52]

The radio frequency pulse scheme for obtaining heteronuclear multiple-quantum filtered 2Q spectra is shown in Figure 10b. A standard three-pulse sequence of duration τ_{exc} is applied to the ^{13}C spins to create ±2Q coherences. The ±2Q coherences are allowed to relax for a variable interval t_1 during which the precession under chemical shifts and *J*-couplings is refocused by a π pulse so that only the relaxation under the stochastic Hamiltonians is operative.

The −2Q part of the spin density operator at the beginning of the evolution interval (time point ① in Figure 10b) is proportional to

$$\rho_{①}^{(-2)} = S_2^- S_3^- = I_1^\alpha S_2^- S_3^- I_4^\alpha + I_1^\alpha S_2^- S_3^- I_4^\beta + I_1^\beta S_2^- S_3^- I_4^\alpha + I_1^\beta S_2^- S_3^- I_4^\beta \quad (34)$$

omitting inessential constants. At the end of the evolution interval (time point ②), the −2Q part of the spin density operator will have evolved into

$$\rho_{②}^{(-2)} = I_1^\alpha S_2^- S_3^- I_4^\alpha \exp(-R_{\alpha\alpha}t_1) + I_1^\alpha S_2^- S_3^- I_4^\beta \exp(-R_{\alpha\beta}t_1) + I_1^\beta S_2^- S_3^- I_4^\alpha \exp(-R_{\beta\alpha}t_1) + I_1^\beta S_2^- S_3^- I_4^\beta \exp(-R_{\beta\beta}t_1) \quad (35)$$

A $\pi/2$ pulse is applied at the ^{1}H Larmor frequency at the end of the interval t_1. This pulse generates heteronuclear multiple-quantum coherences, through transformation properties such as

$$\exp\left\{-i\frac{\pi}{2}I_{1x}\right\} I_1^\alpha \exp\left\{i\frac{\pi}{2}I_{1x}\right\} = \frac{1}{2} - \frac{1}{2i}I_1^+ + \frac{1}{2i}I_1^- \quad (36)$$

$$\exp\left\{-i\frac{\pi}{2}I_{4x}\right\} I_4^\beta \exp\left\{i\frac{\pi}{2}I_{4x}\right\} = \frac{1}{2} + \frac{1}{2i}I_4^+ - \frac{1}{2i}I_4^- \quad (37)$$

The part of the spin density operator containing coherences of order (−2) for the ^{13}C spins and order (±1) for the ^{1}H spins at time point ③ is therefore

$$\rho_{③}^{(-2,\pm1)} = -\frac{1}{4}(I_1^+ S_2^- S_3^- I_4^+ - I_1^+ S_2^- S_3^- I_4^- - I_1^- S_2^- S_3^- I_4^+ + I_1^- S_2^- S_3^- I_4^-) \times \{\exp(-R_{\alpha\alpha}t_1) - \exp(-R_{\alpha\beta}t_1) - \exp(-R_{\beta\alpha}t_1) + \exp(-R_{\beta\beta}t_1)\} \quad (38)$$

Signals passing through ±4Q are selected out by cycling the radio frequency phases of pulse sequence elements before and after time point ③ (see Experimental Section).

The heteronuclear multiple-quantum coherences are converted into antiphase ^{13}C double-quantum coherence by applying a second $\pi/2$ pulse at the proton Larmor frequency. The effect of this can be calculated through transformation properties such as

$$\exp\left\{-i\frac{\pi}{2}I_{1x}\right\} I_1^\pm \exp\left\{i\frac{\pi}{2}I_{1x}\right\} = I_{1x} \pm iI_{1z} \quad (39)$$

The antiphase (−2Q) coherence at time point ④ may therefore be represented by

$$\rho_{④}^{(-2)} = I_{1z} S_2^- S_3^- I_{4z} \{\exp(-R_{\alpha\alpha}t_1) - \exp(-R_{\alpha\beta}t_1) - \exp(-R_{\beta\alpha}t_1) + \exp(-R_{\beta\beta}t_1)\} + \text{other terms} \quad (40)$$

which is converted into in-phase (−2Q) coherences via the heteronuclear $^1J_{CH}$ scalar coupling during the following interval, which has duration $\tau_{CH} = (2J_{CH})^{-1}$. Product operator calculations[53] lead to the expression for in-phase (−2Q) coherence at time point ⑤:

$$\rho_{⑤}^{(-2)} = \frac{1}{4} S_2^- S_3^- \{\exp(-R_{\alpha\alpha}t_1) - \exp(-R_{\alpha\beta}t_1) - \exp(-R_{\beta\alpha}t_1) + \exp(-R_{\beta\beta}t_1)\}$$

neglecting the decay of the coherences during the refocusing interval. This expression is the same as eq 34, except for the additional numerical factors which depend on the differential coherence decay during the interval t_1. A final $\pi/2$ pulse gives

(47) Dalvit, C.; Bodenhausen, G. *Adv. Magn. Reson.* **1990**, *1*, 14.
(48) Boulat B.; Bodenhausen, G. *J. Chem. Phys.* **1992**, *97*, 6040.
(49) Müller, N.; Bodenhausen, G. *J. Chem. Phys.* **1993**, *98*, 6063.
(50) di Bari, L.; Kowalewski, J.; Bodenhausen, G. *J. Chem. Phys.* **1990**, *93*, 7698.
(51) Pekar, J.; Leigh, J. S. *J. Magn. Reson.* **1986**, *69*, 582.
(52) Kay, L. E.; Prestegard, J. H. *J. Am. Chem. Soc.* **1987**, *109*, 3829.
(53) Sørensen, O. W.; Eich, G. W.; Levitt, M. H.; Bodenhausen, G.; Ernst, R. R. *Prog. NMR Spectrosc.* **1983**, *16*, 163.

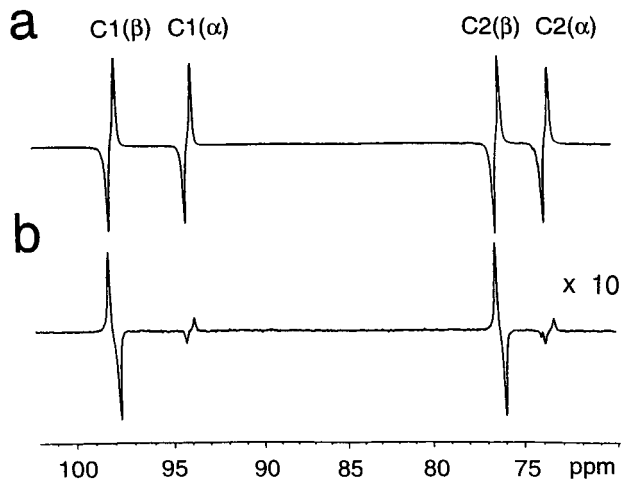

Figure 11. (a) Double-quantum-filtered (2QF) spectrum of [1,2-$^{13}C_2$]-glucose solution obtained using pulse sequence in Figure 10a ($t_1 = 0$). (b) Heteronuclear multiple-quantum-filtered 2QF spectrum of [1,2-$^{13}C_2$]-glucose solution obtained with the pulse sequence in Figure 10b ($t_1 = 0.01$ s). The vertical scale in (b) is 10 times the vertical scale in (a).

the observable signal which is detected in the presence of proton decoupling. As in the usual INADEQUATE experiment, the form of the spectrum is a pair of antiphase doublets. For a series of experiments performed at different values of t_1, the experimental signal amplitudes are given by

$$\alpha(t_1) = \frac{1}{4}A(-e^{-R_{\alpha\alpha}t_1} + e^{-R_{\alpha\beta}t_1} + e^{-R_{\beta\alpha}t_1} - e^{-R_{\beta\beta}t_1}) \quad (42)$$

The differential relaxation effects may therefore be probed by measuring the amplitude of the total signal, rather than by measuring differential spectral peakwidths. This is convenient but reduces the signal by a factor of 2.

When the CSA values of the spins S_2 and S_3 are small, the terms involving CSA in eq 28 can be neglected. The relaxation rate constants of the 2QCs are then related through ($R_{\alpha\alpha} = R_{\beta\beta}$) $\neq$ ($R_{\alpha\beta} = R_{\beta\alpha}$). The expression for signal amplitude becomes

$$a(t_1) = \frac{1}{2}A(-e^{-R_{\alpha\alpha}t_1} + e^{-R_{\alpha\beta}t_1}) \quad (43)$$

In this case, the heteronuclear multiple-quantum filter selects the difference of the inner and outer components of the 2QC multiplets. The signal amplitude depends on the cross-correlation of the pairs of through-space couplings and the sign is determined by the slowly decaying component, and hence on the geometry of the four-spin unit.

This is illustrated for the solution spectra of [1,2-$^{13}C_2$]-glucose in Figure 11. Figure 11a shows the double-quantum-filtered spectrum of the [1,2-$^{13}C_2$]-glucose solution, without the heteronuclear multiple-quantum filter. All doublets have the usual "down-up" configuration. Figure 11b shows the spectrum with the heteronuclear multiple-quantum filter. The signals for the α-anomer are inverted. This spectrum provides a clear distinction between the different geometries at the site of the anomeric carbon, without reference to the values of the chemical shifts or *J*-couplings.

5. Multiple-Quantum-Filtered Signal Trajectories. The experimental dependence of the signal amplitudes on t_1 for the two $^{13}C_2$-labeled glucose anomers is shown in Figure 12. Both curves take the form of a rapid build-up in signal amplitude (for $t_1 < 20$ ms), followed by a relatively slow decay. The heteronuclear multiple-quantum signal amplitudes have opposite signs for the two anomers, as remarked above.

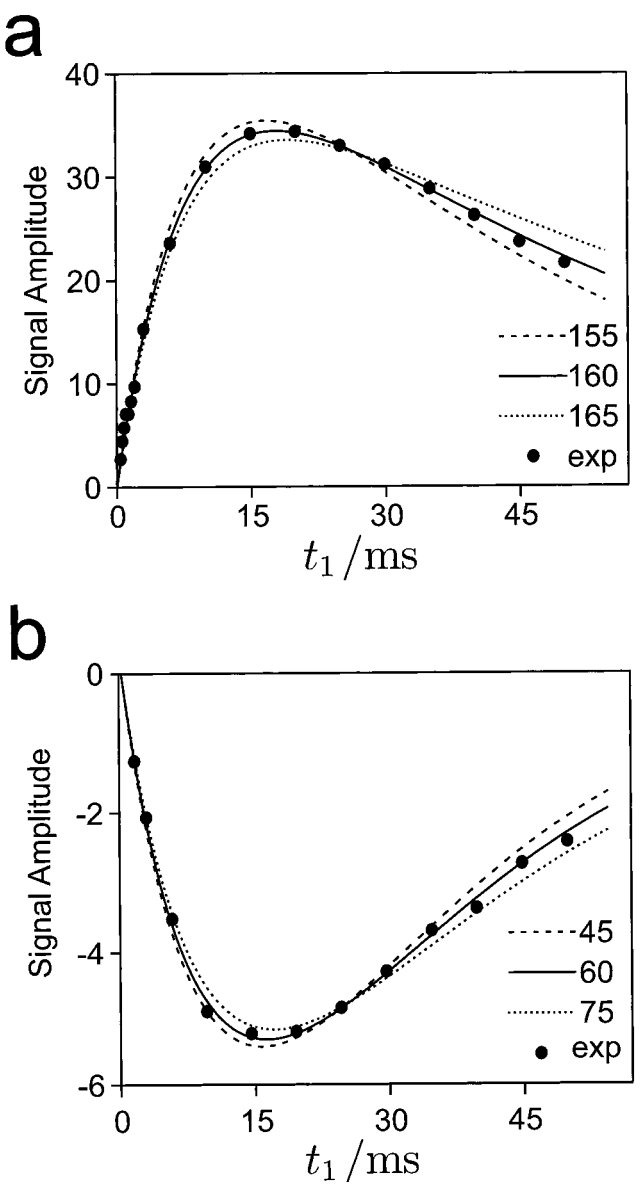

Figure 12. Signal amplitudes as a function of t_1 for β-[1,2-$^{13}C_2$]-glucose (a) and for α-[1,2-$^{13}C_2$]-glucose (b) in a solution-state heteronuclear multiple-quantum-filtered 2Q experiment. The lines are best fit theoretical curves calculated at different torsion angles. The vertical scale is arbitrary but consistent between (a) and (b).

The form of the curves depends on (i) the geometrical parameters in the four-spin unit, i.e., the bond lengths, the bond angles, and the torsion angle ϕ; (ii) the chemical shift anisotropies and the orientation of the principal axes in the molecular frame; (iii) the principal components of the rotational diffusion tensor and the orientation of the rotational diffusion tensor in the molecular frame; (iv) long-range heteronuclear ^{13}C-^1H interactions; and (v) $^1H-^1H$ cross-relaxation, as manifested through nonadiabatic line width contributions given in eqs 31−33.

We investigated the influence of all of these effects on the heteronuclear multiple-quantum-filtered trajectories. Figure 13a shows sets of simulated curves, using increasingly sophisticated models for multiple-quantum relaxation. The geometry and chemical shift anisotropy values are appropriate for the H−C1−C2−H unit in β-glucose.

The simulations were performed for isotropic rotational diffusion, with a rotational correlation time of 9.5 ns, as estimated from ^{13}C T_1 measurements (see above). The principal

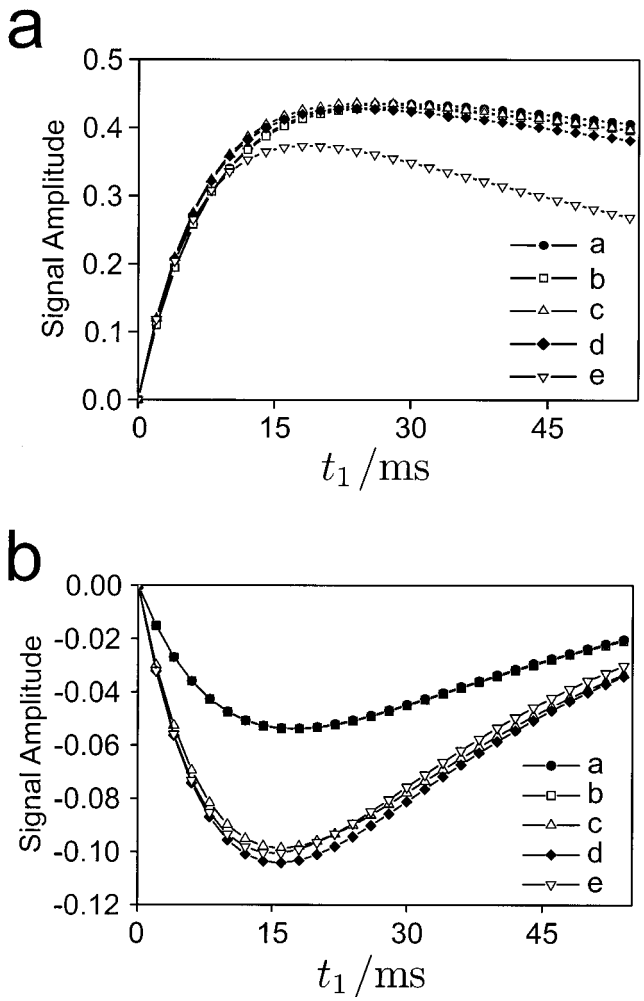

Figure 13. Multiple-quantum-filtered 2Q signal amplitudes as a function of t_1 calculated using eq 42, with $A = 1$. (a) Simulations for β-[1,2-$^{13}C_2$]-glucose; (b) Simulations for α-[1,2-$^{13}C_2$]-glucose. In each plot, the curves are as follows: "a": simulation including only short-range heteronuclear dipolar interactions. "b": simulation using short-range heteronuclear dipolar interactions and ^{13}C CSA. "c": simulation including ^{13}C CSA and all heteronuclear dipolar interactions. "d": simulation including ^{13}C CSA, all heteronuclear dipolar interactions and cross-relaxation between protons I_1 and I_4. "e": simulation including ^{13}C CSA, all heteronuclear dipolar interactions, and all proton−proton cross-relaxation terms. Curves "a" and "b" are nearly superimposed in both plots.

values and orientations of the chemical shift anisotropy tensors were estimated from the single crystal study of methyl-β-D-glucose.[54,55] The chemical shift anisotropies are of the order $\approx$20 ppm.

Curve "a" in Figure 13a shows the signal trajectory taking into account only the short-range heteronuclear dipolar interactions (I_1-S_2 and I_4-S_3). In curve "b" the effect of chemical shift anisotropy is included. The effect is very minor in this case. In curve "c" all heteronuclear dipolar interactions within the four-spin unit were included as well as the CSA. Again the curve is very similar. The small difference between curves "b" and "c" indicates that long-range heteronuclear dipolar interactions only have a minor effect in this geometry.

In curve "d", the nonadiabatic cross-relaxation between proton I_1 and I_4 is also taken into account (the term proportional to $J_{14,14}$ in eq 32). This simulation uses a I_1-I_4 distance of 0.303 nm, as estimated from the crystal structure.[38] The I_1-I_4 cross-relaxation has a minor effect on the signal trajectory. The cross-relaxation between spins I_1 and I_4 and the remaining protons in the molecule, on the other hand, has a rather strong effect (curve "e"). The hydroxyl protons were omitted from this analysis, because they are expected to be in rapid intermolecular exchange.

In Figure 13b, analogous calculations are shown for the α-anomer of [1,2-$^{13}C_2$]-glucose. The curves "a" and "b" are almost superimposed, indicating that chemical shift anisotropy has a very minor effect in this case too. However, curve "c" is displaced strongly from curves "a" and "b", indicating that the long-range heteronuclear interactions within the four-spin unit are relatively important. In particular, the dipole−dipole cross-correlation terms $J_{12,13}$ and $J_{23,34}$, which involve one "long-range" dipolar interaction and one "short-range" dipolar interaction, are comparable to the $J_{12,34}$ cross-correlation term in this geometry. The inclusion of cross-relaxation terms has little further effect, as seen from curves "d" and "e".

These simulations indicate that the main effect on the multiple-quantum-filtered signal trajectories is the dipole−dipole cross-correlation between the one-bond heteronuclear interactions, which has a simple geometric interpretation. However, there is significant interference from several additional terms, such as long-range dipole−dipole cross-correlation terms, and cross-relaxation effects.

Griesinger and co-workers developed methods which involve taking the ratios of peak amplitudes to isolate the most informative cross-correlation effects.[24,26] In a recent paper, the effect of proton−proton cross-relaxation within the four-spin unit was minimized by exploiting the zero-quantum relaxation as well as double-quantum relaxation.[27] In addition, these methods employ proton detection and heteronuclear polarization transfer in order to enhance the sensitivity.

Although these new methods significantly reduce the influence of proton−proton cross-relaxation and other undesirable effects, all methods based on cross-correlation (including the methods described in the present paper) are still sensitive to anisotropic molecular tumbling, as discussed further below.

6. Molecular Torsion Angles and Rotational Correlation Times in Solution. In Figure 12, the experimental heteronuclear mutiple-quantum-filtered signal trajectories for the two anomers are compared with best fit simulations for several molecular torsion angles ϕ. The geometrical parameters for β-glucose are given above; for α-glucose the geometrical parameters used in the simulations are $r_{12} = r_{34} = 0.113$ nm, $\theta_{123} = 109.1°$, and $\theta_{234} = 106.9°$. These parameters correspond to the neutron diffraction structure,[39] except for the short-range C−H distances, as discussed previously. The simulations assume isotropic rotational diffusion with correlation times $\tau_c = 9.5$ ns (for β-glucose) and $\tau_c = 8.4$ ns (for α-glucose). The simulations in Figure 12 neglect chemical shift anisotropy and long-range heteronuclear interactions, but include ^{1}H−^{1}H cross-relaxation. This was done by using the crystal structures to estimate intramolecular ^{1}H−^{1}H distances, excluding hydroxyl protons. In principle, the ^{1}H−^{1}H cross-relaxation rates depend on the geometrical parameter ϕ. However, this dependence is expected to be weak and the cross-relaxation rate constants were fixed in each set of simulations.

Figure 12 shows the best fit simulated curves, obtained by optimizing separately the vertical scale parameter A for each torsion angle ϕ. The H−C1−C2−H torsion angle is determined to be 160° ± 3° for the β-anomer and 60° ± 10° for the

(54) Liu, F.; Phung, C. G.; Alderman, D. W.; Grant, D. M. *J. Am. Chem. Soc.* **1996**, *118*, 10629.
(55) Sastry, D. L.; Takegoshi, K.; McDowell, C. A. *Carbohydr. Res.* **1987**, *165*, 161.

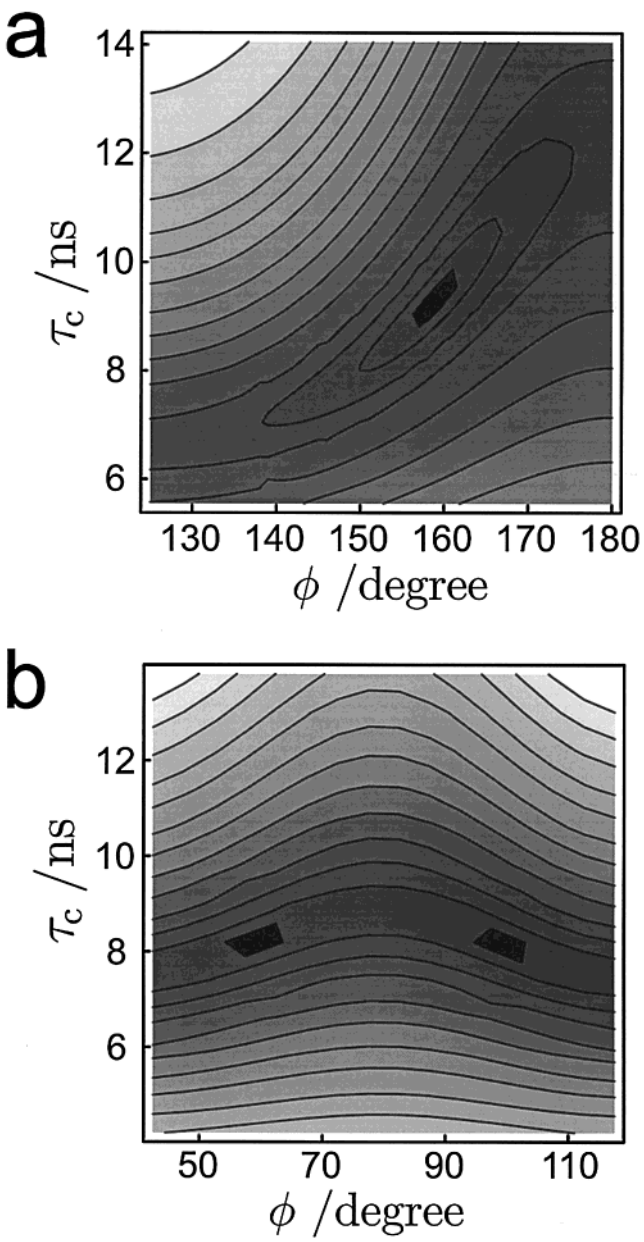

Figure 14. Surface showing the mean square deviation between experimental and theoretical curves in the heteronuclear multiple-quantum-filtered 2Q experiment, for β-[1,2-$^{13}C_2$]-glucose (a) and α-[1,2-$^{13}C_2$]-glucose (b). The mean square deviation is plotted as a function of the rotational correlation time τ_c and the H−C1−C2−H torsion angle ϕ. Dark regions represent minima.

α-anomer. These estimates are modified when rotational anisotropy is taken into account (see below).

The effect of the rotational correlation time on this determination is studied in Figure 14. The figure shows contour plots of the mean square deviation between the theoretical curves and experimental data, as a function of torsional angle and rotational correlation time. Small values of the mean square deviation are indicated by a dark shade. For each value of τ_c and ϕ, the vertical scale factor A was adjusted for the best fit. For β-glucose the calculations span the region of the torsion angle space leading to positive peak amplitudes, whereas for α-glucose the calculations span the regions leading to negative peak amplitudes. The contours indicate that the angular resolution is highest for torsion angles in the vicinity of 180°, being about 5° or better. For the α-anomer the torsion angle resolution is lower, about ±10°. The plots also show that the estimated torsion angle is ambiguous in the range 50°−120°.

The surface for β-glucose, shown in Figure 14a, has a global minimum for a correlation time of $\tau_c = 9.4$ ns and $\phi = 159°$. The determined correlation time is highly consistent with the value of 9.5 ± 0.4 ns obtained from the T_1 measurements.

The surface plot of the mean square deviation for the α-anomer is shown in Figure 14b. This time the surface shows two prominent minima, with the same values of the rotational correlation time, $\tau_c = 8.3$ ns, but at the torsional angles 60° and 100°. The left-hand minimum is close to the H−C1−C2−H torsion angle for crystalline α-glucose, determined by neutron diffraction to be 50.6°.[39] The determined correlation time is highly consistent with the value of 8.4 ± 0.3 ns, obtained from T_1 measurements for nonlabeled glucose under identical conditions.

These results indicate that the geometrical estimation does not require independent knowledge of the rotational correlation time.

A potential source of error in the geometry determination is the rotational anisotropy of the molecule. It is known that cross-correlation effects are sensitive to rotational anisotropy,[56,57] so an interpretation in terms of isotropic rotation could be inaccurate. We have therefore assessed the influence of anisotropic rotational diffusion on the torsion angle estimation.

It is difficult to take into account anisotropic rotational diffusion because the principal values of the rotational diffusion tensor (D_{xx},D_{yy},D_{zz}) and the orientational angles Ω_{MD}, are unknown. Nevertheless, it is possible to constrain the possible values by using the measured spin−lattice relaxation time constants for the ring carbons. We proceeded by selecting a large number of diffusion tensor orientations Ω_{MD}, by varying each Euler angle α_{MD}, β_{MD}, and γ_{MD} in steps of 10°. For each of these orientations, the parameters D_{xx}, D_{yy}, and D_{zz} were optimized to obtain the best fit to the T_1 values of the ring ^{13}C sites in glucose. The parameter sets giving the best fits to the T_1 data were selected (root mean square $\approx 10^{-3}$ or less). For each of the parameter sets which was consistent with the experimental T_1 data, we analyzed the results of the heteronuclear multiple-quantum-filtered 2Q experiment by generating coordinates corresponding to a range of torsion angles and optimizing the parameter A in eq 43. The mean torsion angle determined for several orientations of the diffusion tensor was 159° with a standard deviation of ±10° for β-glucose. For the α-anomer, the mean torsion angle is 57° with a standard deviation of ±7°. This analysis indicates that rotational anisotropy adds some uncertainty to the torsion angle estimation in solution. Nevertheless, it is still possible to obtain accurate torsional angle information, at least in this case.

The influence of rotational anisotropy on the torsion angle estimation might be much larger for extended molecules such as oligonucleotides. The only sure way to eliminate this effect is to immobilize the molecules by freezing and then employ the solid-state version of the experiment as described above.

The H−C1−C2−H torsion angle for glucose in solution may be compared with those obtained by diffraction measurements in crystals. For the α-anomer, neutron diffraction of crystals[39] gives a value of 50.6° and HCCH-2Q-HLF NMR in solution gives a value of 57° ± 7°. For the β-anomer; X-ray diffraction of β-glucose gives an estimate of 170°,[38] whereas HCCH-2Q-HLF NMR in solution gives an estimate of 159° ± 10°. The

(56) Werbelow, L. G.; Grant, D. M. *Adv. Magn. Reson.* **1977**, *9*, 189.
(57) Werbelow, L. G. In *Encyclopedia of NMR*; Grant, D. M., Harris, R. K., Eds.; Wiley: New York, 1996; Vol. 6, p 4072.

slight structural differences in the two phases may be due to flexibility of glucose molecules in solution, or possibly a slight twist due to hydrogen bonding with the solvent.

V. Conclusions

We demonstrated the potential of experiments involving evolution/relaxation of 2QCs under correlated dipolar interactions for providing molecular geometrical information on carbohydrates in both the solution and the solid phases. These experiments distinguish different anomers by aiming directly at their geometrical differences. The basic strategy is very similar in the solid state and in solution. In both cases the torsion angle resolution is particularly high in the vicinity of a trans geometry for the H−C−C−H moeity. The determined torsion angle is ambiguous and the resolution is lower in the range around 50° − 120°.

We conducted solid-state HCCH-2Q-HLF experiments on the two glucose anomers and obtained values which agree well with crystallographic determinations. We also demonstrated that the solid-state HCCH-2Q-HLF experiment is applicable to HCCH moieties with carbons which are not directly bonded. These solid-state experiments may be used to obtain long-range structural information such as the relative orientations of bonds, ring pucker, and the determination of conformations across glycosidic linkages.

We also performed a detailed analysis of cross-correlated double-quantum relaxation in solution. The determined H−C1−C2−H torsion angles for the α- and β-anomers of glucose in solution differ from solid-state angles by about 10°. The rotational correlation time of the molecules was obtained independently from the decay curves. For glucose, rotational anisotropy only has a small effect on the torsion angle estimate.

These experiments are feasible routes for obtaining geometrical information on macromolecular carbohydrates and glycoconjugates. The solid-state HCCH-2Q-HLF experiment has been applied to a 41 kD membrane protein,[16] so macromolecular carbohydrate systems and nucleic acids of this size should also be within reach. The solution state HCCH-2Q-HLF experiments are also applicable to macromolecules, once the sensitivity of the experiment is enhanced by implementing additional coherence transfer steps.[24] However, the solution state experiments are limited to molecules which have correlation times less than around 10 ns in solution, and the accuracy of the torsion angle estimates may be degraded by the possibility of rotational anisotropy. The solid-state experiments do not have these limitations.

We are planning to use the techniques described in this paper to investigate carbohydrate−carbohydrate interactions, as part of an investigation of cell−cell recognition mechanisms.

VI. Experimental Section

1. Solid State NMR. Sample. The sample of [1,2-$^{13}C_2$]-glucose was purchased from Cambridge Isotope Laboratories and used without further purification or recrystallization. The quoted labeling levels were 99% for the two sites.

The sample of methyl-α-D-[1,3-$^{13}C_2$]-glucose (1,3-mag) was prepared as follows. A sample of [1,3-$^{13}C_2$]-glucose was obtained from Omicron Biochemicals, IN. The magnetically diluted sample of 1,3-mag was prepared by refluxing 15 mg of [1,3-$^{13}C_2$]-glucose and 145 mg of unlabeled glucose in 4 mL of acidified methanol. The α-anomeric form was crystallized from the solution by addition of a seed crystal of methyl-α-glucopyranoside.

2Q-HLF Experiment. The experiments were performed on a CMX-400 infinity spectrometer at a magnetic field of 9.4 T. A standard 4 mm triple-resonance probe was used. Experiments were carried out at ambient temperature. For the experiments on [1,2-$^{13}C_2$]-glucose, the sample spinning frequency was $\omega_r/2\pi = 5223$ Hz and a cross-polarization time of 1.0 ms was used. The double-quantum excitation interval was 547 μs. For each increment of t_1, 32 transients were collected with a waiting interval of 100 s between each experiment. For the experiments on 1,3-mag, the sample spinning frequency was set to 5416 Hz and the cross-polarization time was 3.0 ms. The double quantum excitation interval was 2637 μs. For each increment of t_1, 32 transients were collected, separated by a waiting interval of 50 s between each transient. In both cases, the ^{13}C reference frequency was set to the mean of the isotropic Larmor frequencies of the two labeled sites. The interval t_1 was increased from 0 to τ_r in steps of $\tau_{MREV8}/4$, where τ_{MREV8} is the duration of a full MREV8 cycle.

2. Solution NMR. The solution experiments were carried out on a 1 M solution of [1,2-$^{13}C_2$]-glucose in glycerol with D_2O as external lock. The temperature was regulated to 303 K. The viscosity of the solvent was 934 mPa·s at 298 K.

2D Double Quantum Experiment. Experiments were performed on a Varian unity INOVA spectrometer at a magnetic field of 9.4 T using a standard 10 mm high-resolution probe. The double-quantum excitation interval τ_{exc} was 10.9 ms. This corresponds to $1/(2J_{CC})$, where $J_{CC} = 46$ Hz is the one-bond carbon−carbon coupling constant between the two labeled sites. Proton decoupling was turned off during the evolution interval. Proton decoupling during excitation of the 2QC and signal acquisition was achieved by employing WALTZ-16.[58] The decoupler frequency was set to the center of the proton spectrum. A 2D signal matrix $s(t_1,t_2)$ was built up by using 512 increments of t_1. The 2D data sets, 512 × 7808 points were zero filled to 4 K × 16 K before Fourier transformation. Absorption phase spectra with frequency discrimination in the ω_1 dimension were obtained by the Time Proportional Phase Incrementation (TPPI)[59] procedure. The desired coherence transfer pathways were selected by employing the phase cycle, $\phi_{1C} = \text{floor}(q/4)2\pi/2$, $\phi_{2C} = \text{floor}(q/8)2\pi/4$, $\phi_{3C} = 0$, $\phi_{4C} = 2\pi q/4$, where $q = 0,1,2...$ is the transient counter. The post-digitization phase[60] ϕ_{dig} was adjusted to satisfy $\phi_{1C} - 2\phi_{2C} + \phi_{4C} + \phi_{dig} = 0$. Floor($x$) denotes the largest integer which is not larger than x. The basic 32-step cycle is followed by an overall phase cycle of four steps for quad image supression.

Heteronuclear Multiple-Quantum-Filtered 2Q Experiment. The pulse sequence is shown in Figure 10b. Excitation of ±2QC is achieved as described above. The interval τ_{CH} was 3.5 ms. This corresponds to $1/(2J_{CH})$ where $J_{CH} = 143$ Hz is the carbon−proton coupling constant. Extensive phase cycling was employed to select the desired coherence transfer pathways. The phase cycling employed is $\phi_{1C} = 2\pi q/4$, $\phi_{2H} = \text{floor}(q/4)2\pi/4$, $\phi_{2C} = \text{floor}(q/16)2\pi/8$, $\phi_{3C} = \text{floor}(q/128)2\pi/8$, $\phi_{4C} = 0$, and $\phi_{dig} = -2\phi_{1C} + 4\phi_{2C} - 2\phi_{2H} - 4\phi_{3C}$. A total of 1024 transients were accumulated for each t_1 increment.

Acknowledgment. This research was supported by the Natural Sciences Research Council of Sweden and the Göran Gustafsson Foundation for Research in the Natural Sciences and Medicine. We wish to thank Ole G. Johannessen and Torbjörn Astlind for their help, and Omicron Biochemicals for the sample of [1,3-$^{13}C_2$]-glucose.

JA9910863

(58) Shaka, A. J.; Keeler, J.; Frenkiel, T.; Freeman, R. *J. Magn. Reson.* **1983**, *52*, 335.

(59) Marion, D.; Wüthrich, K. *Biochem. Biophys. Res. Commun.* **1983**, *113*, 967.

(60) Levitt, M. H. *J. Magn. Reson.* **1997**, *126*, 164.